

INSTITUTE OF
PAPER CHEMISTRY
Appleton, Wisconsin

**HYDRODYNAMIC DRAINAGE THROUGH
SHEETS OF CONSTANT RESISTANCE**

II. DRAINAGE AT LINEAR FOILS

Project 2570

Report Five

A Progress Report

to

MEMBERS OF GROUP PROJECT 2570

May 29, 1968

THE INSTITUTE OF PAPER CHEMISTRY
Appleton, Wisconsin

HYDRODYNAMIC DRAINAGE THROUGH SHEETS OF CONSTANT RESISTANCE

II. DRAINAGE AT LINEAR FOILS

Project 2570

Report Five

A Progress Report

to

MEMBERS OF GROUP PROJECT 2570

May 29, 1968

MEMBERS OF GROUP PROJECT 2570

ALLIS-CHALMERS MANUFACTURING COMPANY

APPLETON WIRE WORKS CORP.

BELOIT CORPORATION

CONSOLIDATED PAPERS, INC.

CONTAINER CORPORATION OF AMERICA

EASTMAN KODAK COMPANY

FIBREBOARD CORPORATION

THE GLIDDEN COMPANY

INTERNATIONAL PAPER COMPANY

KIMBERLY-CLARK CORPORATION

KNOWLTON BROTHERS

LONGVIEW FIBRE COMPANY

THE MEAD CORPORATION

OXFORD PAPER COMPANY

RIEGEL PAPER CORPORATION

SCOTT PAPER COMPANY

UNION CAMP CORPORATION

WEST VIRGINIA PULP AND PAPER COMPANY

WEYERHAEUSER COMPANY

TABLE OF CONTENTS

Page

SUMMARY	1
INTRODUCTION	3
DESCRIPTION OF EQUIPMENT AND EXPERIMENTS	6
DATA AND DATA REDUCTION	11
COMPARISON WITH THEORY	29
DISCUSSION OF RESULTS	33
DEMONSTRATION OF PREDICTION	36
CONCLUSIONS	39
ACKNOWLEDGMENTS	42
NOMENCLATURE	42
LITERATURE CITED	45
APPENDIX I. DRAINAGE AT A FOIL	46
APPENDIX II. DEFLECTION OF A RIGID WIRE UNDER TENSION	57
APPENDIX III. ESTIMATE OF EFFECT OF FRICTION AND DISPLACEMENT THICKNESS	61
APPENDIX IV. EFFECT OF SPEED ON WIRE TENSION	65

THE INSTITUTE OF PAPER CHEMISTRY
Appleton, Wisconsin

HYDRODYNAMIC DRAINAGE THROUGH SHEETS OF CONSTANT RESISTANCE

II. DRAINAGE AT LINEAR FOILS

SUMMARY

Experiments on suction distribution and drainage of water through a fabric-wire composite resistance and under variations of the rest wire tension are described. The raw drainage data were reduced by correction for gravity drainage and the backwash effect of a scraper's leading edge and converted by use of scale factors obtained from an analysis. Drainage at linear foils is analyzed on the assumption of streamline flow in the nip and by taking the deflection of a slack wire into account. The resulting integral equation for the suction distribution was solved numerically for the case of a straight wire (infinite wire tension) and found to be in partial agreement with Taylor's solution for complete mixing in the nip. An approximate solution for finite wire tension is also presented which satisfies the boundary condition and the integral equation at two points.

A representation of the experimental data in a manner suggested by theory shows good qualitative agreement with the predictions by the approximate solution reflecting, more specifically, the typical effect of wire tension, foil angle, etc., on drainage performance. By use of a "piston" velocity of foil drainage it is possible to enter and to make use of a graph (of so far limited extent) of the predicted drainage and to obtain the mean drainage velocity for a given wire tension. Computed rates of drainage come (on the average) within 15% of the measured data as compared with overpredictions in the order of 50% by means of the ideal (infinite wire tension) theory. The main cause for a good portion of the remaining discrepancies between data and prediction is seen in the applied correction for the scraper effect, which is presently under a

complementary study. Other possible sources of error have given rise to investigations (see Appendices II-IV) of (1) the effect on the analysis of a rigid wire under tension, (2) estimated viscous effects on nip flow, and (3) the contribution of centrifugal force and wire deflection to wire tension.

INTRODUCTION

In the first report of this series on Hydrodynamic Drainage (1), preliminary results for a 2-inch table roll and for a 2.5° plane foil were presented. The process of obtaining reliable data was much simplified by the use of layers of 200-mesh nylon cloth substituting for wet fiber mats in the 50-g./m.² basis weight range. Up to three layers of that material were found incompressible under permeating flow rates as high as 200 cm.³/sec./unit area. An approximate analysis of the drainage data suggested that Taylor's nip flow theory when extended to accommodate a power law of flow through the porous sheet permits a much better prediction of table roll drainage than earlier attempts had indicated. Our observation was restricted to cases where the effects of finite wire tension are negligible.

Experiments and analyses to be described in this report deal with drainage at plane foils in the range of wire speeds of $300 < \underline{U}_w < 1400$ f.p.m. Preliminary tests had shown that the original flow distributor could not be adapted to produce straight and uniform jets at slice velocities $\underline{U}_j > 1000$ f.p.m.. Also, the then available maximum flow rate of 69 USGPM per foot width posed too close an upper limit to the operational speed at which drainage at the foils could still be reliably observed. The supply system was therefore changed and a new flow distributor installed as described in more detail in one of the following sections. Two plane foils with machined inclinations of 2.5° and 4.9° and set at these same angles to the wire at rest were investigated. Varying the wire tension within the possibilities of the High-Speed Hydrodynamic Suction Device (HSHSD) had a significant effect on both suction distribution and rate of drainage. The desire for a more quantitative understanding of these data made it necessary to analyze the drainage process on a new basis and to include the effect of wire deflection. The analyses by G. I. Taylor, J. Bergstroem, and the

one presented in Appendix I have the common feature that in setting up the flow equations for the nip, viscous effects are either neglected [as in references (6) and (7)] or estimated by assuming a constant friction factor [as in reference (4)], which was done in order to make an analytical solution of the momentum balance equation possible. The treatment of these problems on the basis of the Navier-Stokes equations [which were shown (8) to reduce to one equation under these conditions] would undoubtedly be more realistic and preferable, but also greatly increases the difficulties encountered in preparing numerical solutions. A rather lengthy computer program for the "boundary layer" equation of foil drainage is on cards, but hopes of getting quick answers have been in vain. Much advantage was gained by dealing with the nonviscous theory, and attempts to solve the "boundary layer" equation will be resumed as soon as it is convenient.

Here, a theory of foil drainage through a deflecting slack wire screen of zero stiffness is presented, based on Taylor's (6) streamline model of flow in the wire-foil nip. Results obtained both through numerical solution and dimensional analysis of the equations serve as the basis of discussion of the data. Some of the measured suction profile data for wire speeds $\underline{U}_w > 700$ f.p.m. showed a distinct temporary increase of pressure located between initial and peak suction which cannot be explained in terms of the slack fabric model of the wire employed. As demonstrated the more realistic model of a stiff wire under tension would be capable of describing the actual wire deformations more accurately. Its use in combination with the flow equation would change the predicted suction distribution in the desired direction. No urgent need was seen at this time to carry out the drainage analysis on this basis because of satisfactory agreement between data and predictions.

The fact that the streamline theory of nip flow as applied in the main analysis ignores frictional effects could mean the prediction of higher suction

throughout and, for that reason, predicted drainage rates greater than measured. Displacement thickness of the foil boundary layer and the reduction of suction due to viscous friction at the foil surface are therefore estimated on the basis of reasonable assumptions. Although the results seem to be significant, they must be looked at with reservation because of the implicit limitations of the approach.

Adjusting the wire tension when the machine is at rest determines solely the initial level from which changes of tension occur due to speed-dependent effects of changing operational conditions. As a preparation for industrial applications the effect of machine speed is analyzed to some degree which allows estimates to be made. For the speed range of the present data, no immediate need was seen to apply such a correction to the rest of the wire tension.

The arrangement of the material and results to be presented in the following chapters was made in the hope that it would help to make this account of a difficult subject matter more readable. We proceed from descriptions of the equipment used and of the data directly to the comparison with the predictions without presenting their theoretical basis first, as is often the practice elsewhere. An effort has also been made to keep the various analyses of Appendices I-IV as independent from one another as possible.

DESCRIPTION OF EQUIPMENT AND EXPERIMENTS

The notes of this chapter serve to describe changes of and additions to the HSHSD [as previously described in an earlier report (2)] which became necessary in order to improve its utility in the range of operational speeds greater than 900 f.p.m., or for other reasons.

The Teflon coating of the Al sheet serving as a "forming board" had to be replaced by a bone-hard rubber cover because of a "blooming" corrosion of the metal wherever the coating was or became porous.

Although the fabric used in the initial phase of the experimental work had performed quite well, the problems of maintaining it moist and the considerable disturbance at the seam dictated selection of another material. The suppliers of commercial filter fabrics were contacted and several grades of material were evaluated for their permeability and moisture stability characteristics. The final choice fell on an Olefin-monofilament fabric obtained from Filtration Fabrics Inc., East Moline, Ill., and identified by the number SNA-E800-APO. Instead of fastening the cloth to the wire by stitching, as was previously done, a two-component adhesive epoxy resin (E-7) from Teck Kits proved to have sufficient bond strength between wire and fabric to hold it in place. The fabric was cut to length in place on the wire with a heated knife and the two surfaces held together with an approximately 3/4-in. wide strip of adhesive tape. The joint was then bonded at various spots across the width of the wire with epoxy resin.

The previously observed periodic spouting during passage of the seam through the slice jet area is now greatly reduced at wire speeds up to 1400 f.p.m. A joint without tape would still be preferable, in view of the nonsteadiness which it introduces in an otherwise perfectly steady drainage process.

Some mechanical improvements were also made. A 20-h.p. drive unit was installed in order to provide adequate power for the entire velocity range of interest. A water tank and centrifugal pump were connected to the system to provide water recirculation capacity and thus higher volumetric feed rates to the system.

The performance of the flow spreader with regard to uniformity of the slice jet became very unsatisfactory at velocities greater than 1000 f.p.m. A duct of essentially constant cross section, it suffered increasingly from "inertial separation" of the flow on both sides which caused local starvation of the fabric-wire system at the foil with a resultant decrease in drainage. Attempts to correct the nonuniformity of the discharge by adjustable vanes inside the spreader failed. A sketch of the new flow distributor is shown in Fig. 1. Seven baffles in alternating up-and-down position and with adjustable ends serve to distribute the water entering the box via a manifold consisting of two 2-in. diameter pipes uniformly over the machine width. The jet velocity, U_j , can be regulated by a valve in the supply system, and the uniformity of the water layer thickness delivered to the wire by adjusting the discharge nozzle. The length of the nozzle was dictated by the need to minimize furrowing of the exiting jet as a result of the violent turbulent action inside the box. An even longer nozzle could be used if necessary to improve the surface smoothness of the jet. The distributor is made of stainless steel plates and sheet material in a semiwelded (i.e., partly screwed) construction. The top plate can be removed for the adjustment of the baffle ends. The new unit gave a much more uniform volume distribution of water and has overcome most of the difficulties encountered with the old inlet.

In addition to the 2.5° foil, for which preliminary data were given in the first report on drainage, a new foil of 4.9° inclination was machined from a

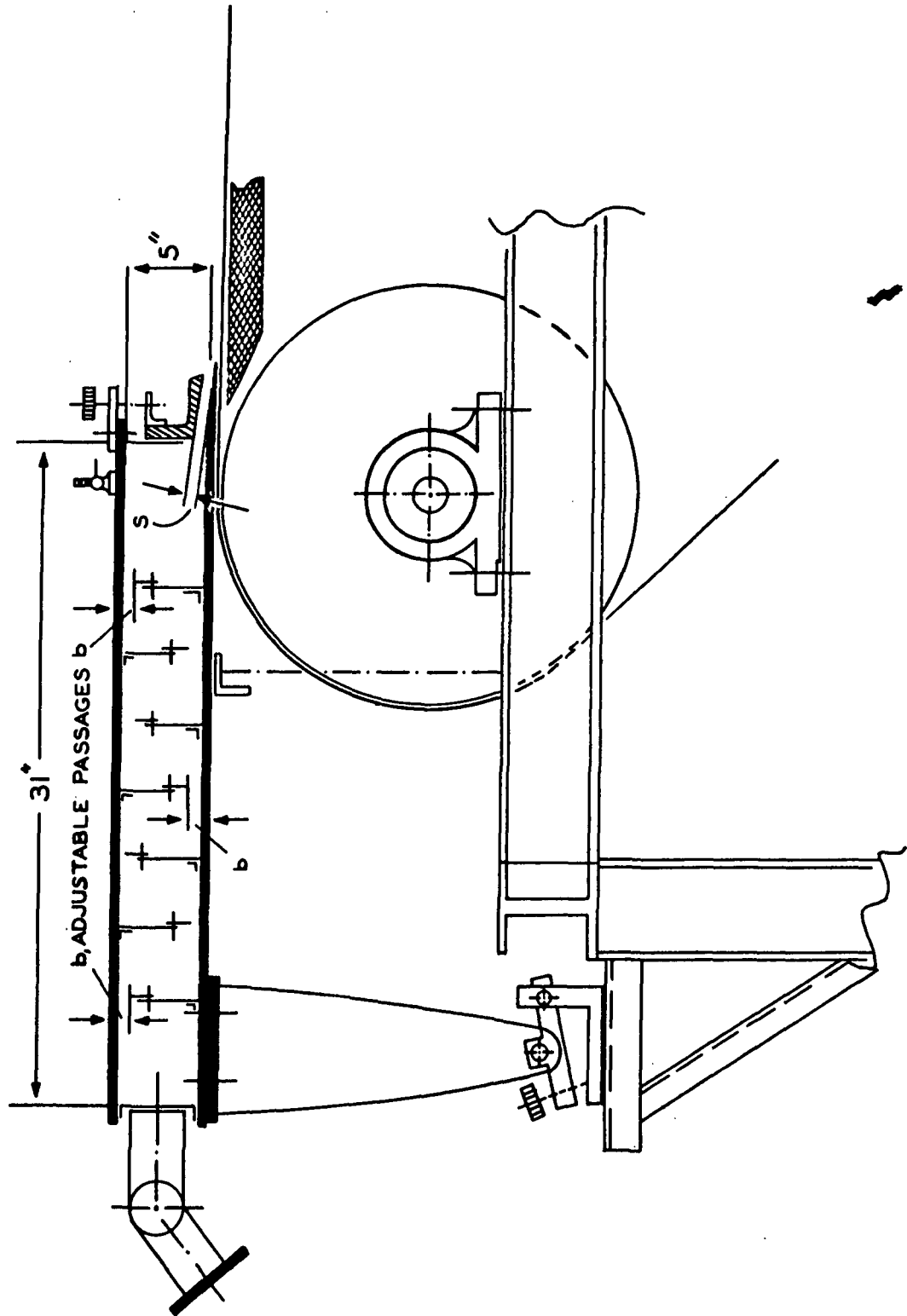


Figure 1. Sketch of New Flow Distributor

2 by 2-in. stainless steel angle and was equipped with suction taps. The arrangement of the tap holes corresponds to the one previously reported--the first one, in machine direction, again being located at the break between the inclined surface and the flat wire support behind the leading edge. The first series of experiments with the 4.9° foil did bring to light an interesting phenomenon. At wire speeds $\underline{U}_w > 900$ f.p.m., nip flow began to separate from the foil surface at certain isolated spots which could be clearly identified as the tap holes. The number of separation points depended on the wire tension applied, but generally increased with speed. Vibrations, as introduced by hammering against the foil, eliminated the separation temporarily until revived, with the passage of the seam being the apparent trigger. This separation upset the reading of pressure profiles, but did not introduce a serious error in the drainage measurements until the area involved had become significant, i.e., extended over most of the tap holes. Various possibilities of removing this limitation were considered, among them: the replacement of the hydrostatic suction measurement by employing surface-flush strain gages and reducing the seam width as the triggering disturbance. But ultimately, the situation was accepted as the present limitation for the range of data to be covered. Depending on wire tension and wire speed, local flow separation also took place at the 2.5° foil. Here it was possible to extend the range of separation-free wire speeds by reducing the tap hole diameter from 1/16 to 1/32 in.

Although there appeared to be sufficient water available to satisfy the drainage requirements even at a slice opening of 0.2 in., the drainage data for this opening were inconsistent at some of the higher wire speeds. Apparently, locally starved conditions due to a slice flow with relatively deep furrows cause streaky separation of nip flow from the foil. Such conditions are readily visible from both the top and bottom sides of the wire.

Spouting as frequently observed on industrial machines was not a problem in the range of these experiments. Some spouting occurred from the landing jet and, under the condition of a near-dry fabric surface, from the leading edge of the drainage pan scraper at speeds $\underline{U}_w > 1500$ f.p.m. Spouting from the foils did not occur at these speeds. The linear foil seems to restrict those changes of the wire curvature which cause the sort of accelerations known to be responsible for the spouting phenomenon.

DATA AND DATA REDUCTION

In essence, the experimental program was the same as that described in Report Four (1). It included a series of preceding flow measurements in order to determine the viscous and inertial resistance coefficients \underline{a}' and \underline{b}' , respectively, as well as the exponent \underline{c} in the pressure drop-flow rate relationship

$$\Delta P = p = \mu a'v + b'\rho^{1-c} v^{2-c} \quad (1)$$

holding for the wire-fabric composite as used throughout the foil drainage experiments. The data are shown in Fig. 2. At a city water temperature of 25°C., these coefficients turned out to be

$$c = 0; \quad a_0 = \mu a' = 0.263 \text{ g}_f \text{ sec.}/\text{cm.}^3; \quad b_0 = \rho b' = 0.0333 \text{ g}_f \text{ sec.}^2/\text{cm.}^4 \quad (2)$$

for a total range of superficial velocities $0 \leq \underline{v} \leq 200 \text{ cm./sec.}$ For later use of the previously introduced and more convenient expression

$$p = K\underline{v}^m \quad (3)$$

instead of Forchheimer's form (1) of the pressure drop-flow rate relationship, the drainage coefficient, \underline{K} , and the exponent \underline{m} must be known in terms of \underline{a}_0 , \underline{b}_0 , and \underline{v}_1 , i.e., the range of expected superficial drainage velocities. For this purpose, the simultaneous transcendental equations (49) and (50) of Report Four must be solved numerically under variation of \underline{v}_1 . The result of this computation is shown in Fig. 3 where both \underline{K} and \underline{m} are plotted vs. \underline{v}_1 , valid for \underline{a}_0 and \underline{b}_0 values adjusted to a water temperature of 5°C., which was the prevailing water temperature of the foil drainage experiments to be described. Compatible values of \underline{K} and \underline{m} are those for equal

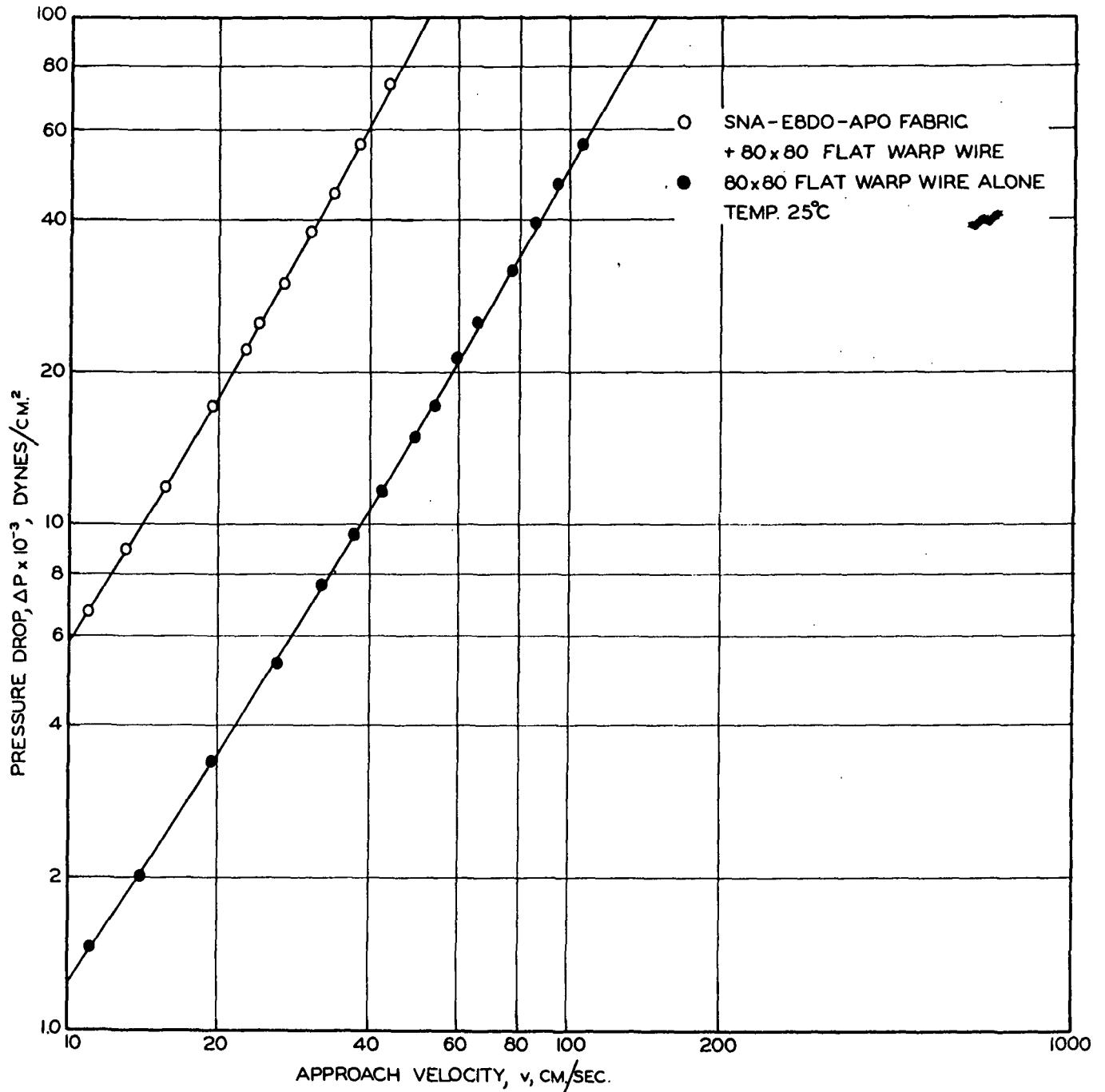


Figure 2. Pressure Drop-Velocity Data for the Wire and Wire-Fabric Composite

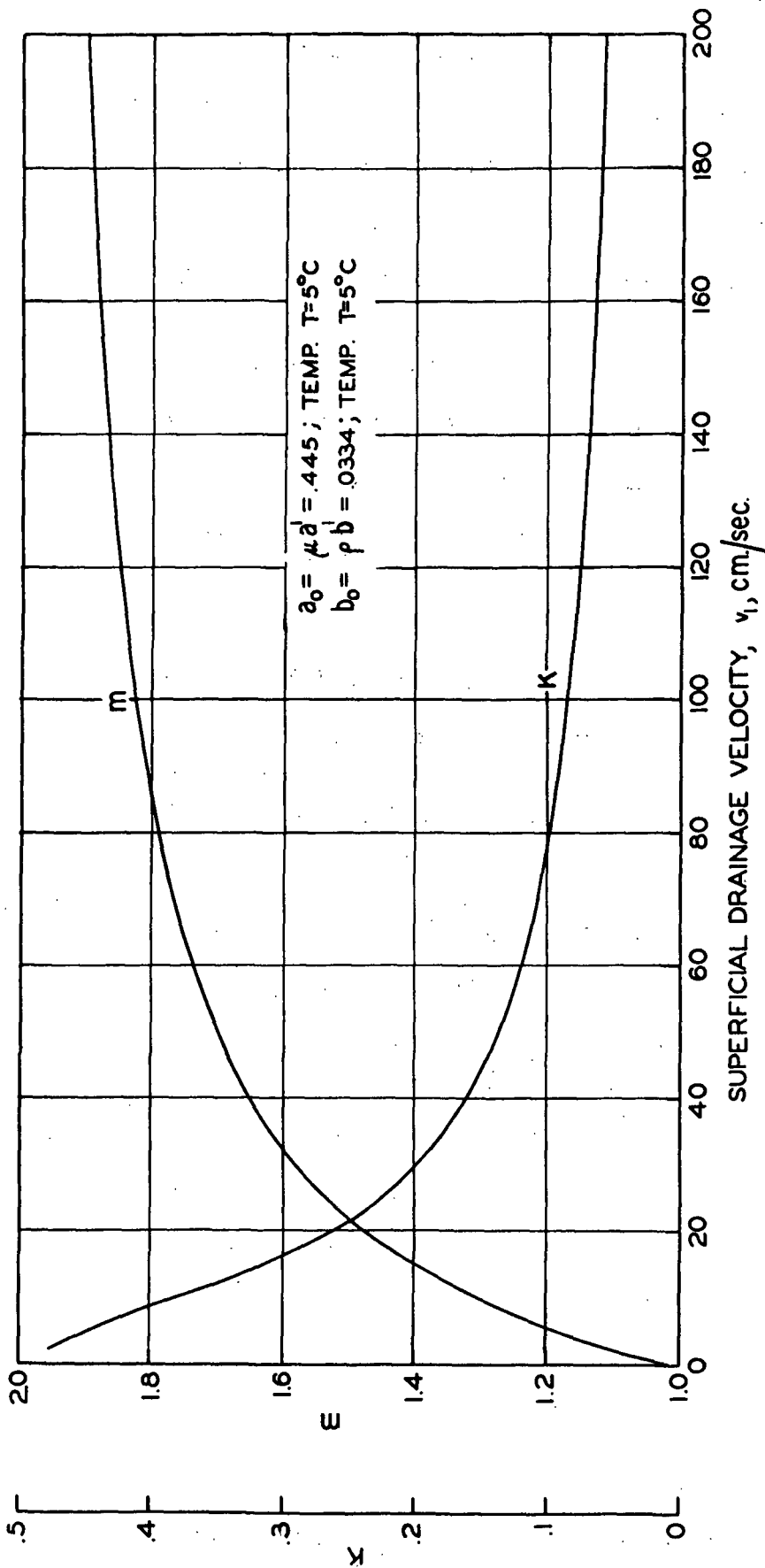


Figure 3. Drainage Coefficient, K , and Exponent, m , for the Wire-Fabric Resistance Data of Fig. 2

superficial drainage velocities, v_1 . A chart of compatible values is then obtained by plotting K vs. m as was done to get the plot of Fig. 4. For values of m closer to unity, drainage flow is primarily viscous and $K \rightarrow a_0$. For values of m closer to 2, energy losses proportional to the square of the superficial velocity are becoming more significant and $K \rightarrow b_0$.

Three slice openings and three wire tensions were evaluated for drainage performance. Apparatus and method for obtaining the wire tension at rest were the same as described in Report Four. As an example, Fig. 5 shows the static load-wire deflection diagram for wire tension G used during one of the 4.9° foil drainage runs.

A full wire speed-drainage rate profile was established for each volumetric discharge rate from the inlet including that for matched velocities.

Figure 6 is a typical plot of the raw drainage data as obtained for this study. The selection of the slice opening was arbitrary as all the data follow this general form. The parameter involved in the family of curves is the jet velocity, U_j . The problem of the flow separation mentioned earlier necessitated a rather comprehensive development of the curve at each jet velocity.

Data were obtained for matching velocities up to 1400 f.p.m. over three wire tensions for a 4.9° and the previously used 2.5° foil. Figures 7 and 8 show the drainage at matching jet and wire velocities for the two foils at two selected levels of wire tension. The contribution of gravity drainage is evidenced by the shift in level for each of the three slice openings. Additional data were collected for a table roll of 4-in. diameter, which will be presented in another report. For reasons of the experimental set-up as described in Report Four, each drainage rate represents the sum of three contributions: from hydrodynamic suction at the drainage element, from permeation due to gravity drainage between the

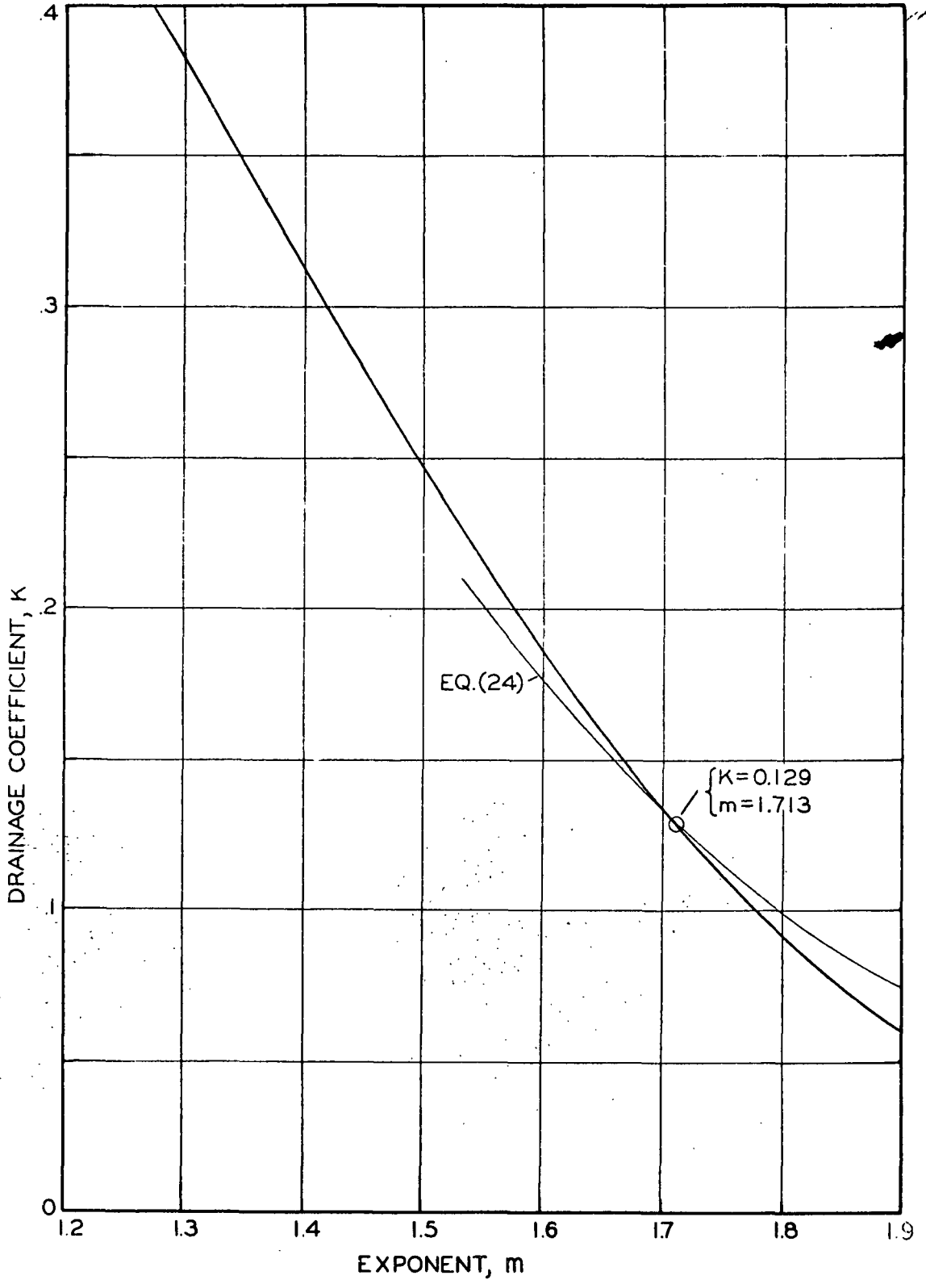


Figure 4. Compatible \underline{K} and \underline{m} Values for the Wire-Fabric Composite Resistance of Fig. 2

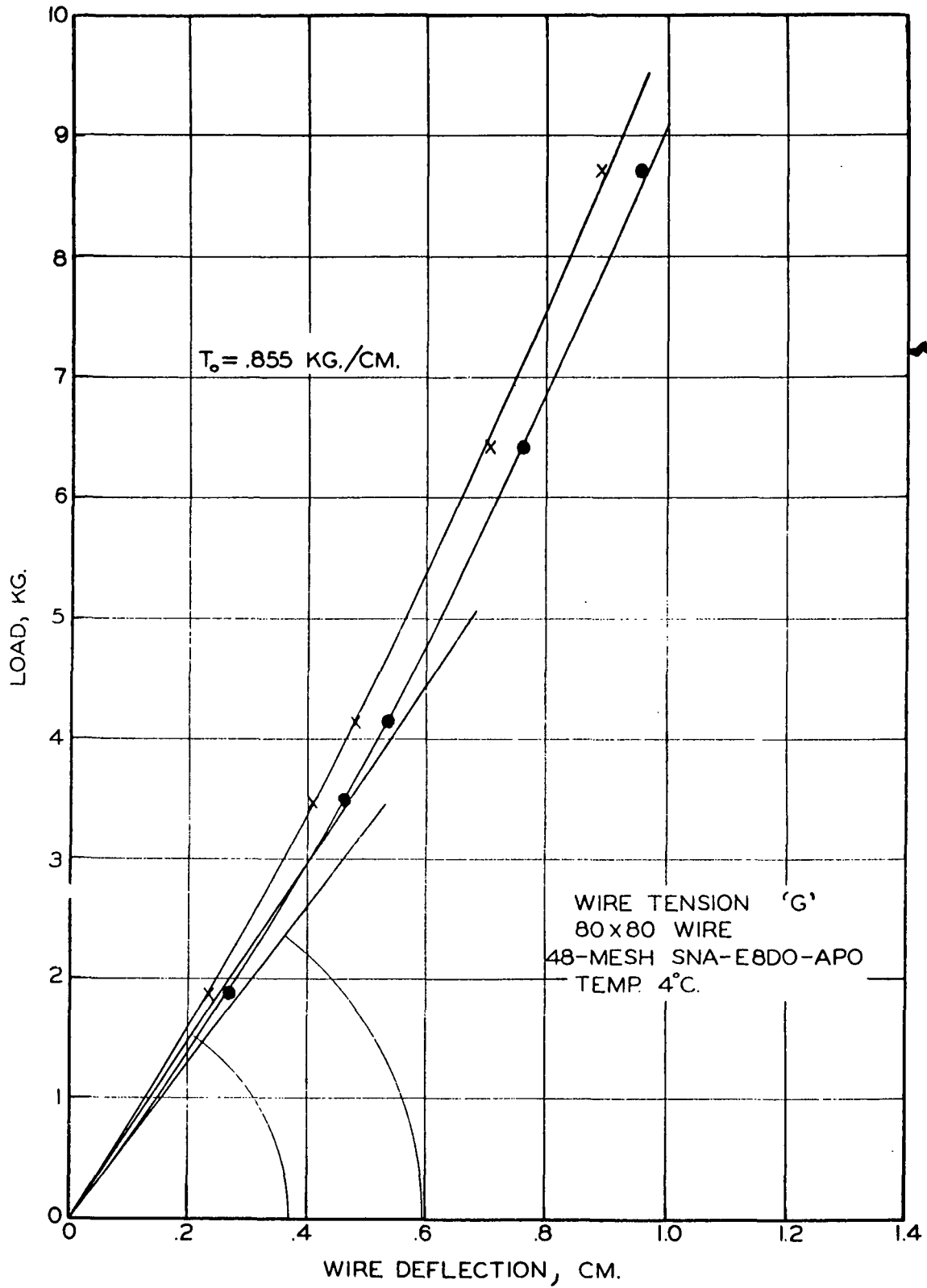


Figure 5. Static Load-Wire Deflection Plot

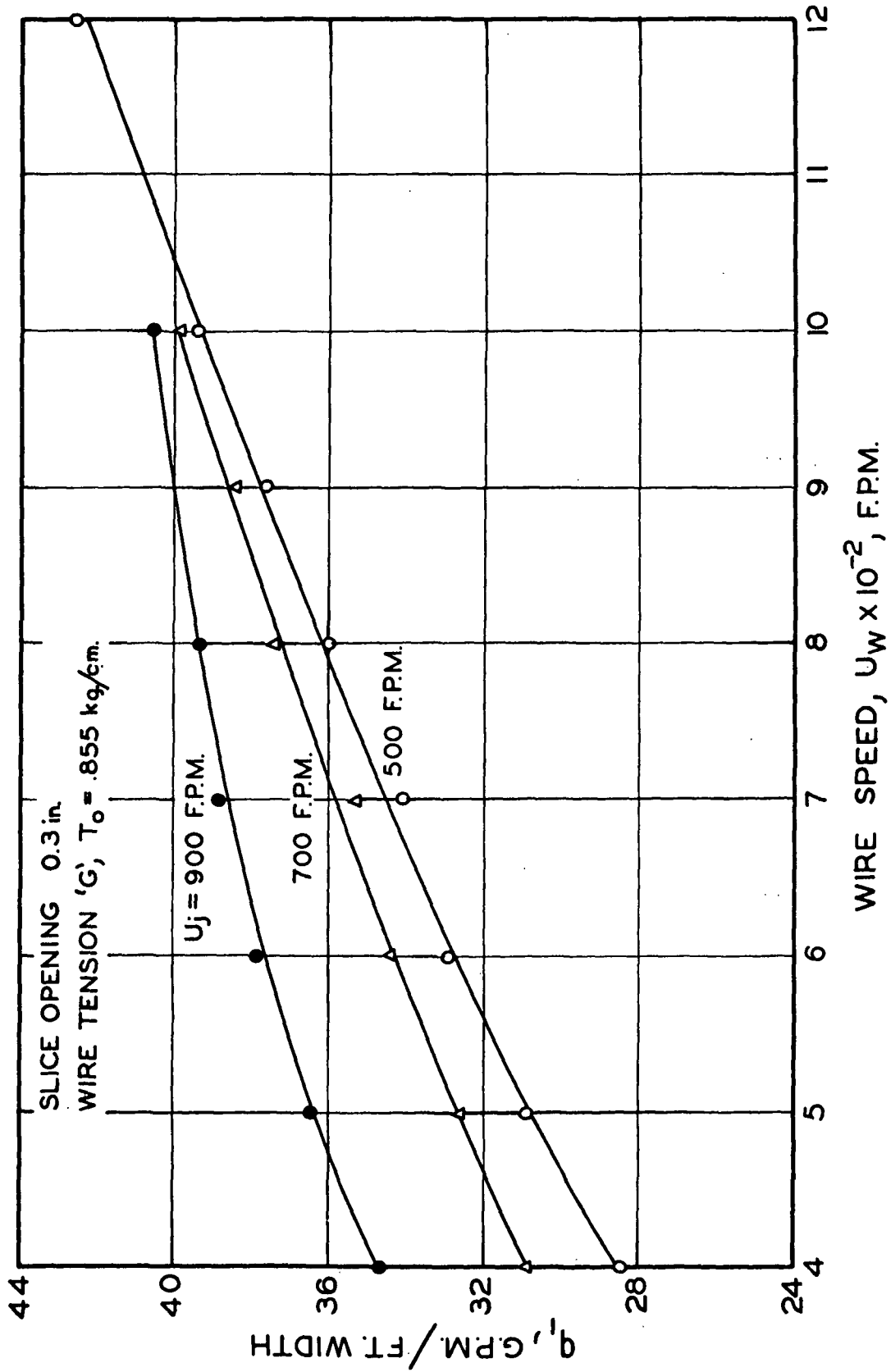


Figure 6. Measured Rate of Drainage, q_1 , for Varying Wire Speeds, U_w

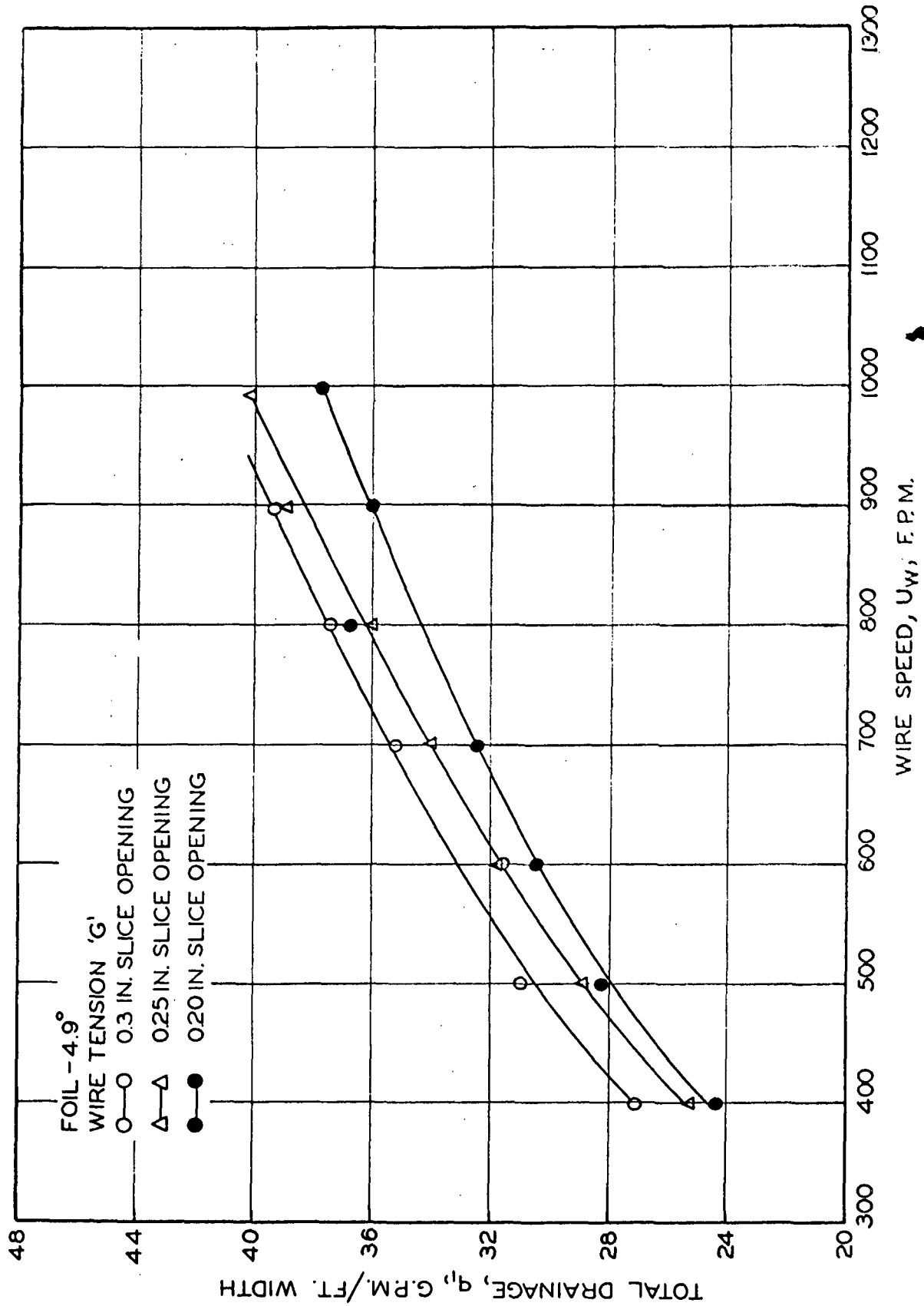


Figure 7. Measured Drainage Rate, q_t , at Matching Jet and Wire Speeds

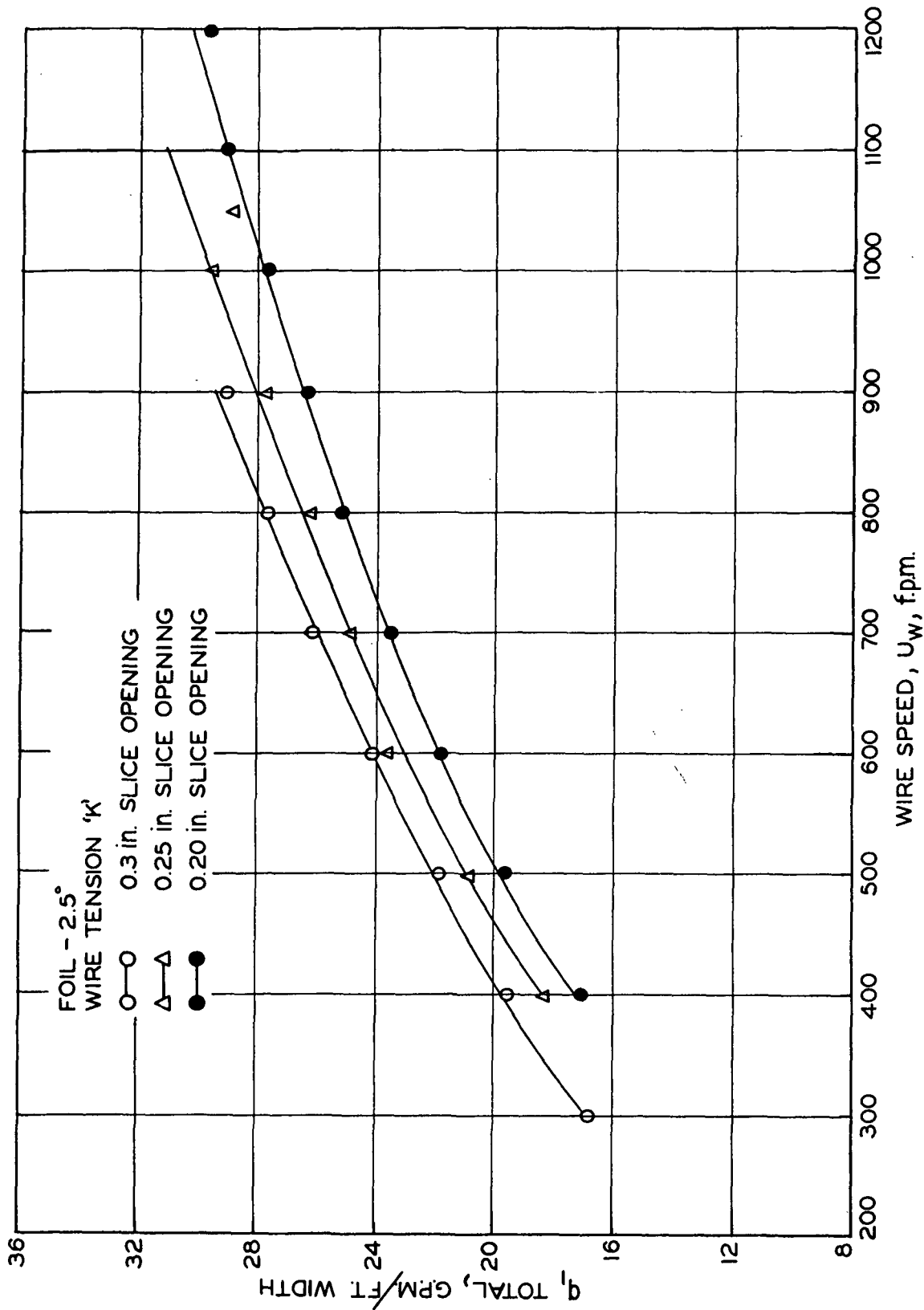


Figure 8. Measured Drainage Rate, q_1 : at Matching Jet and Wire Speeds, U_w

trailing edge of the suction element and the scraper, and from the backwash effect of the scraper's leading edge. Let \underline{q}_d , \underline{q}_g , \underline{q}_s denote these rates, and let \underline{q}_1 be the total rate discharging from the drainage pan; then the rate due to the action of the drainage element alone becomes

$$\underline{q}_d = \underline{q}_1 + \underline{q}_s - \underline{q}_g \quad (4)$$

where, as previously shown (1), drainage due to gravity over a free length at an original head \underline{h}_0 can be predicted by evaluating the formula

$$\underline{q}_g = \underline{h}_0 \underline{U}_w \{1 - \exp[\rho g L_2 / (\mu a' U_w)]\} \quad (5)$$

with \underline{U}_w as the speed of travel of wire and water and \underline{L}_2 as the free length of wire between two foils (see App. I). The underlying assumption here is that flow through fabric and wire is primarily viscous. A theory of the scraper effect was given in Report Four (1) based on this same assumption which is a rather arbitrary one in this case and made only in order to make the problem strictly tractable. Again, it was found that the final Equation (38) of that report tended to overpredict the scraper effect and thus make the drainage rate, \underline{q}_d , at the foils too large. The scraper effect was therefore re-analyzed for the case of a resistance law according to Equation (3). The problem becomes considerably more involved and an approximate solution was considered sufficiently accurate for the present purpose. It could be shown that the rate \underline{q}_s at which the water when arriving at the scraper leading edge at a rate $\underline{y}_0 \underline{U}_w$ is being forced back into the wire is computed by means of the following formula:

$$\underline{q}_s = \underline{y}_0 \underline{U}_w \phi \quad (6)$$

where

$$\Phi = \frac{\rho(1 - \cos\gamma)U_w^{2-m}}{\rho(1 - \cos\gamma)U_w^{2-m} + (K/m)C^{m-1} \sin^m \gamma} \quad (7)$$

and where ρ = specific mass of the water, γ = scraper leading edge angle, and $C = 0.372$. As can easily be verified, $\underline{q}_s \rightarrow 0$ when $\gamma \rightarrow 0$ and increasing with increasing angle γ . For $\underline{m} \rightarrow 1$ and $\underline{K} \rightarrow \underline{\mu a}'$, the above equation assumes the same form which could be obtained by use of Equation (38) of Report Four. From a mass balance of the water hanging under the wire one obtains

$$v_o U_w = q_d + q_g \quad (8)$$

as the rate at which this water approaches the scraper's leading edge, and from a balance for the upper side of wire and fabric,

$$\varphi s U_w = h_o U_w + q_d \quad (9)$$

with \underline{s} = "headbox" slice opening and $\varphi \approx 0.98$. Upon combining Equations (4), (5), (6), (8), and (9), the overall balance Equation (4) yields as the rate of hydrodynamic drainage

$$q_d = \exp[\rho g L_2 / (\underline{\mu a}' U_w)] \left\{ \frac{q_1}{1 - \Phi} - \varphi s U_w (1 - \exp[-\rho g L_2 / (\underline{\mu a}' U_w)]) \right\} \quad (10)$$

where Φ is given by Equation (7). Provided all appearing bits are known, Equation (10) can be applied in order to reduce the measured drainage rates, \underline{q}_1 (i.e., the raw data) by the amounts of gravity drainage and rate of backwash. The only numbers not immediately known are the \underline{K} and \underline{m} values of the wire-fabric composite because the range, \underline{v}_1 , of the superficial backwash velocity is not known. Very probably, \underline{v}_1 is directly proportional to the wire speed, \underline{U}_w , but the approximate method applied in arriving at Equation (6) did not have to be very specific regarding this point. Pending the outcome of a separate

investigation of the scraper effect, \underline{K} and \underline{m} were estimated and assumed independent of wire speed. $\underline{K} = 0.25$ and $\underline{m} = 1.5$ were the chosen values which, according to Fig. 3, correspond to a superficial backwash velocity $\underline{v}_1 = 22$ cm. per sec. The foil drainage data as obtained after reduction are shown in Fig. 9 where smooth curves are drawn through the arithmetic mean value of three drainage rates, \underline{q}_d , for each wire speed, \underline{U}_w , according to the three slice openings used. Small residual variations of \underline{q}_d were found nonsystematic with respect to \underline{s} and may be considered due to experimental error. An immediate effect of wire speed on foil drainage is apparent, likewise of the angle of inclination, α : the greater the angle, α , the more water is drained. For both foils, drainage increases with increasing wire tension, regardless of wire speed.

When the water discharge velocity at the headbox nozzle was the same as the wire speed and equilibrium was reached, readings, \underline{p} , of the manometers connected to the tap holes of the foils were also taken. The suction data, plotted in the nondimensional form $f(\underline{x}/\underline{L}) = 2\underline{p}/\rho\underline{U}_w^2$, are represented in Fig. 10-12 for the 4.9° foil under three wire tensions, $\underline{T}_D = 1.995$; 1.5 ; 0.855 kg_f. per cm., and in Fig. 13 for the 2.5° foil at the wire tension, $\underline{T}_D = 2.39$ kg_f. per cm. Attempts with the 2.5° foil to repeat the pressure readings for lower wire tensions were unsuccessful because of at least partial flow separation at the taps.

All suction profiles have certain common features: The initial value of suction is finite and decreasing with wire speed. The suction maxima for the 4.9° foil are considerably less than known from table-roll experiments (3) and very much less in the case of the 2.5° foil. While their location wanders away from the leading edge, their amount also decreases with increasing wire speed, as shown in Fig. 10-12 for the large-angle foil. In the case of the 2.5° foil and the wire tension of $\underline{T}_D = 2.4$ kg_f./cm. (Fig. 13), maximum suction increases with

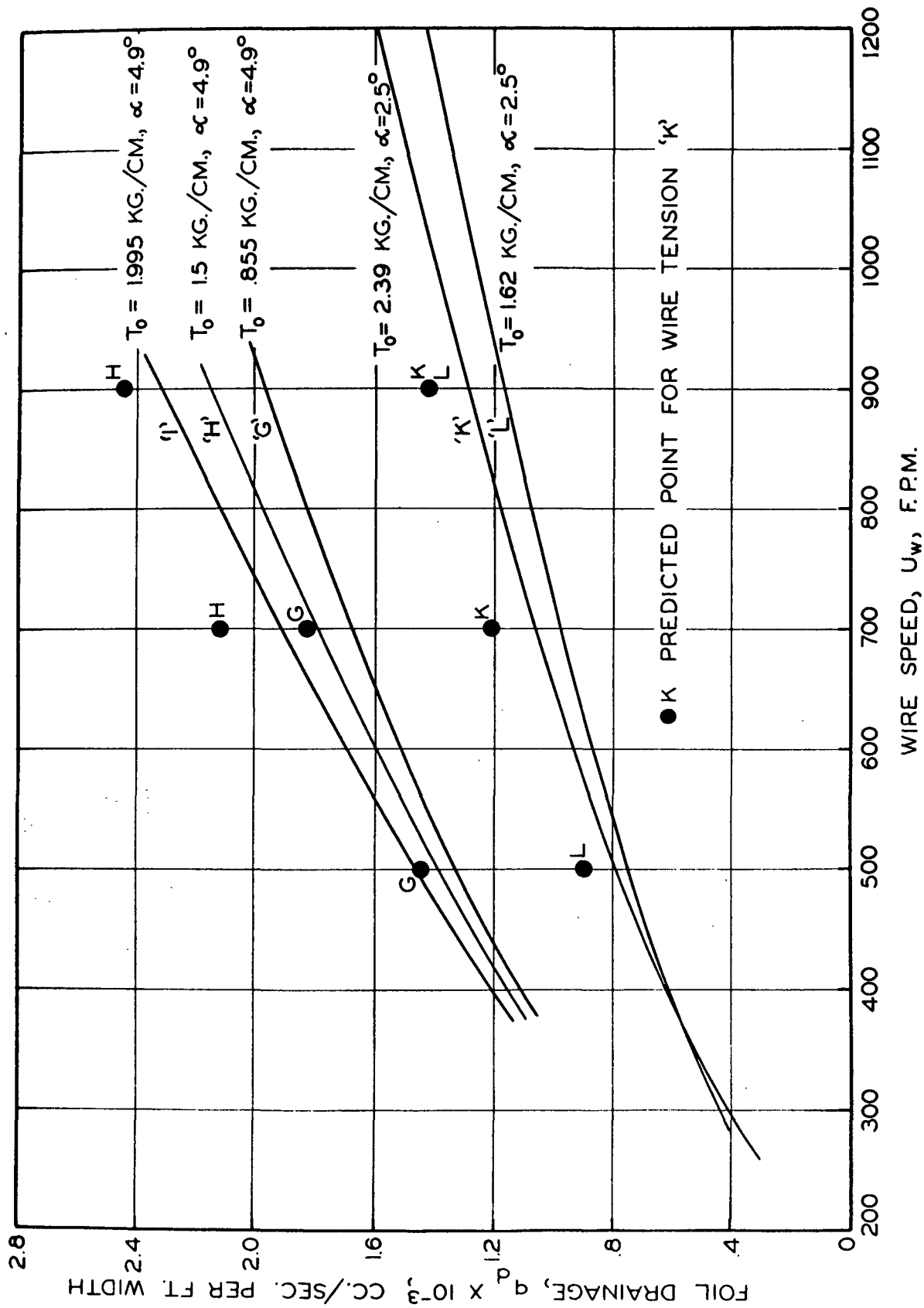


Figure 9. Drainage, q_d , at Two Linear Foils for Matching Jet and Wire Speeds

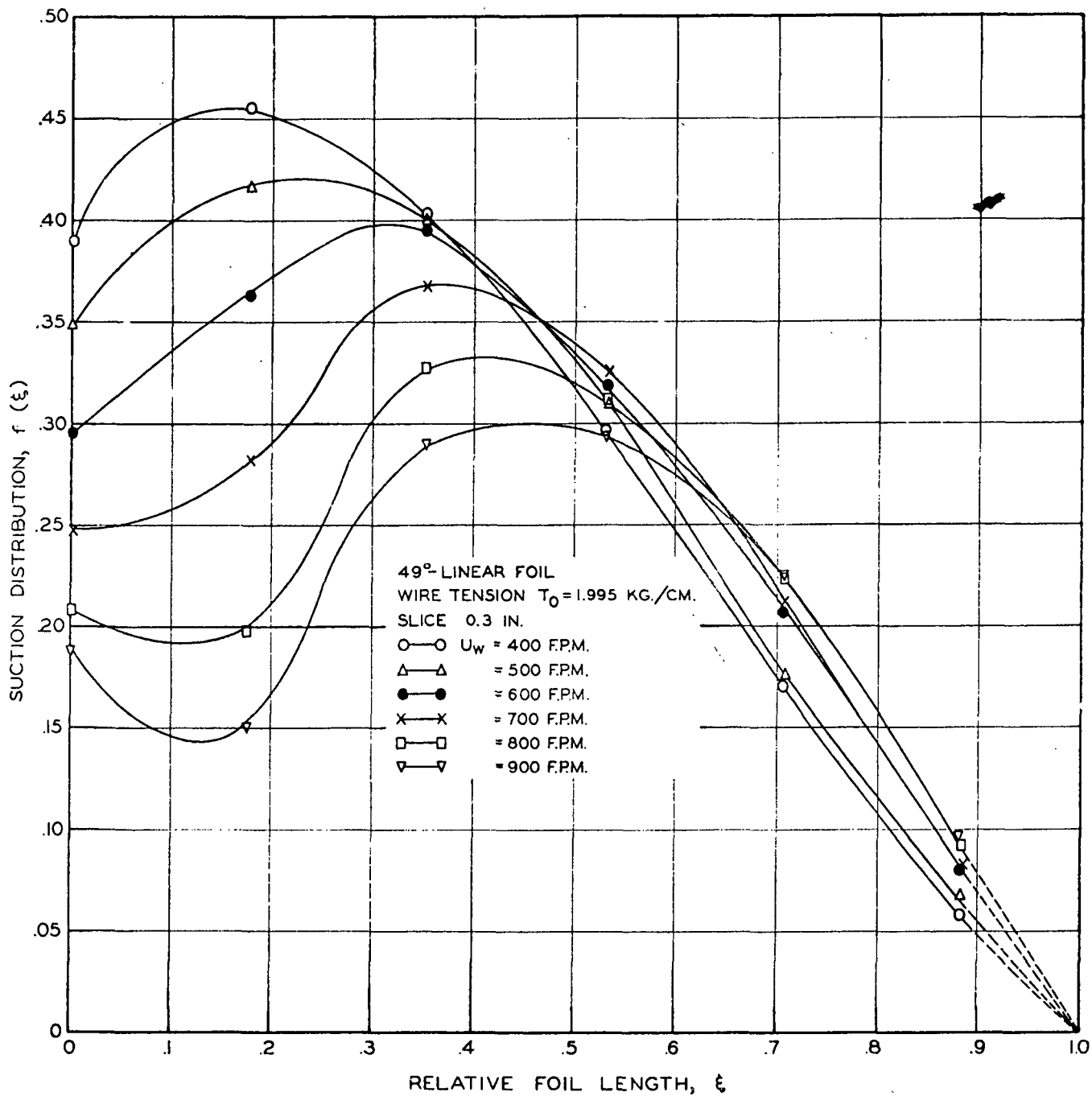


Figure 10. Distribution of Suction at a Foil for Varying Wire Speeds, U_w

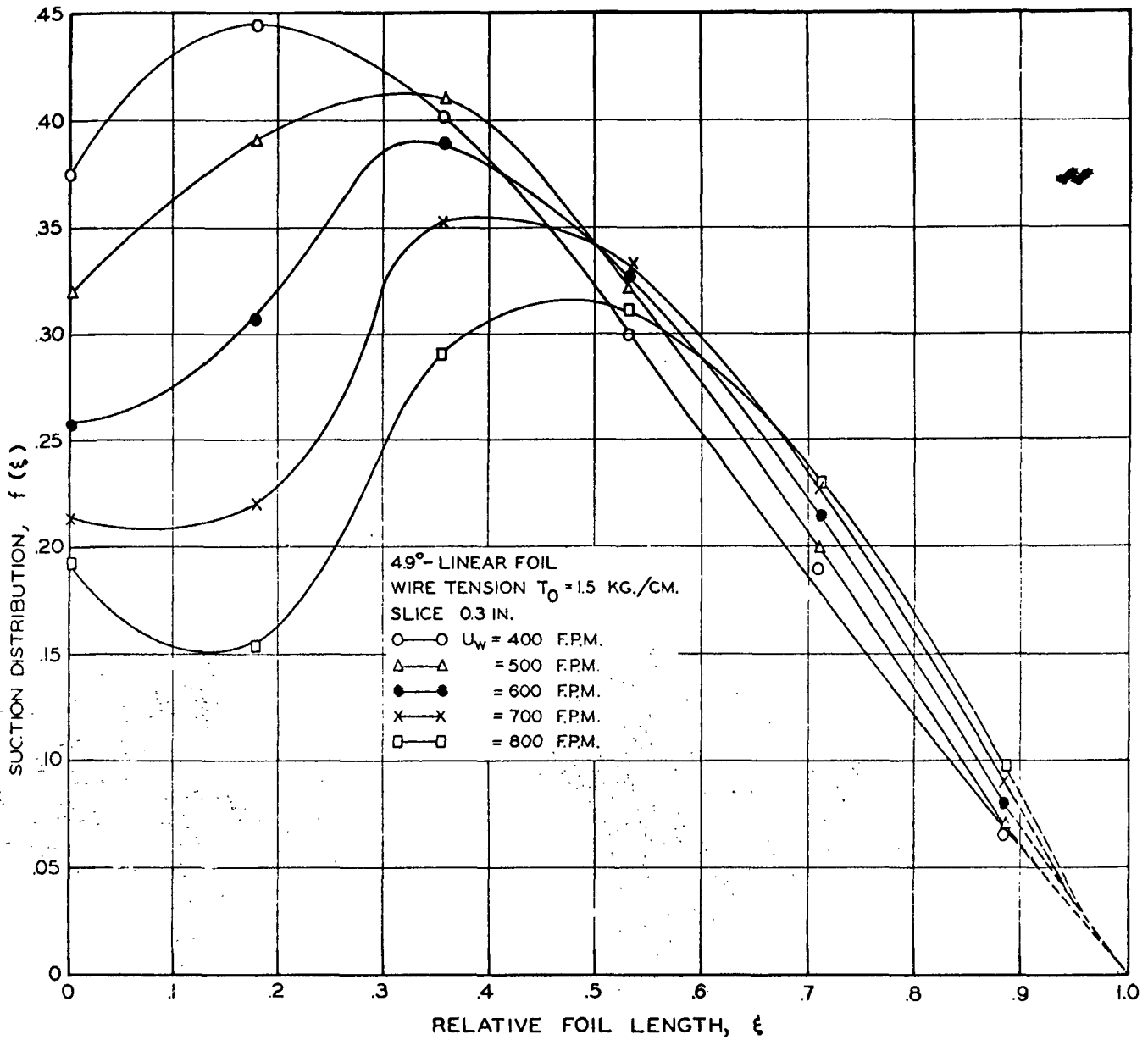


Figure 11. Distribution of Suction at a Foil for Varying Wire Speeds, U_w

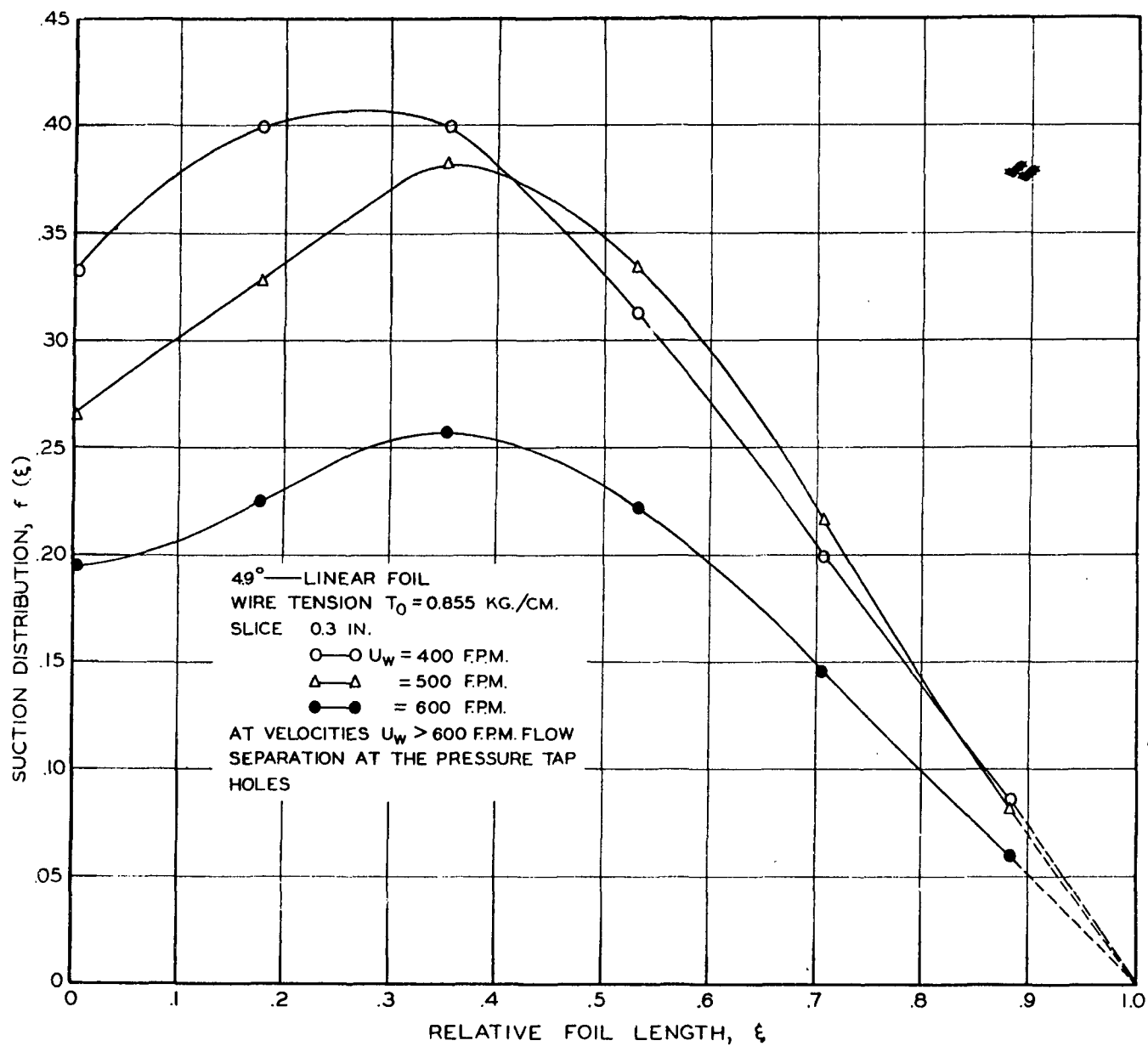


Figure 12. Distribution of Suction at a Foil for Varying Wire Speeds, U_w

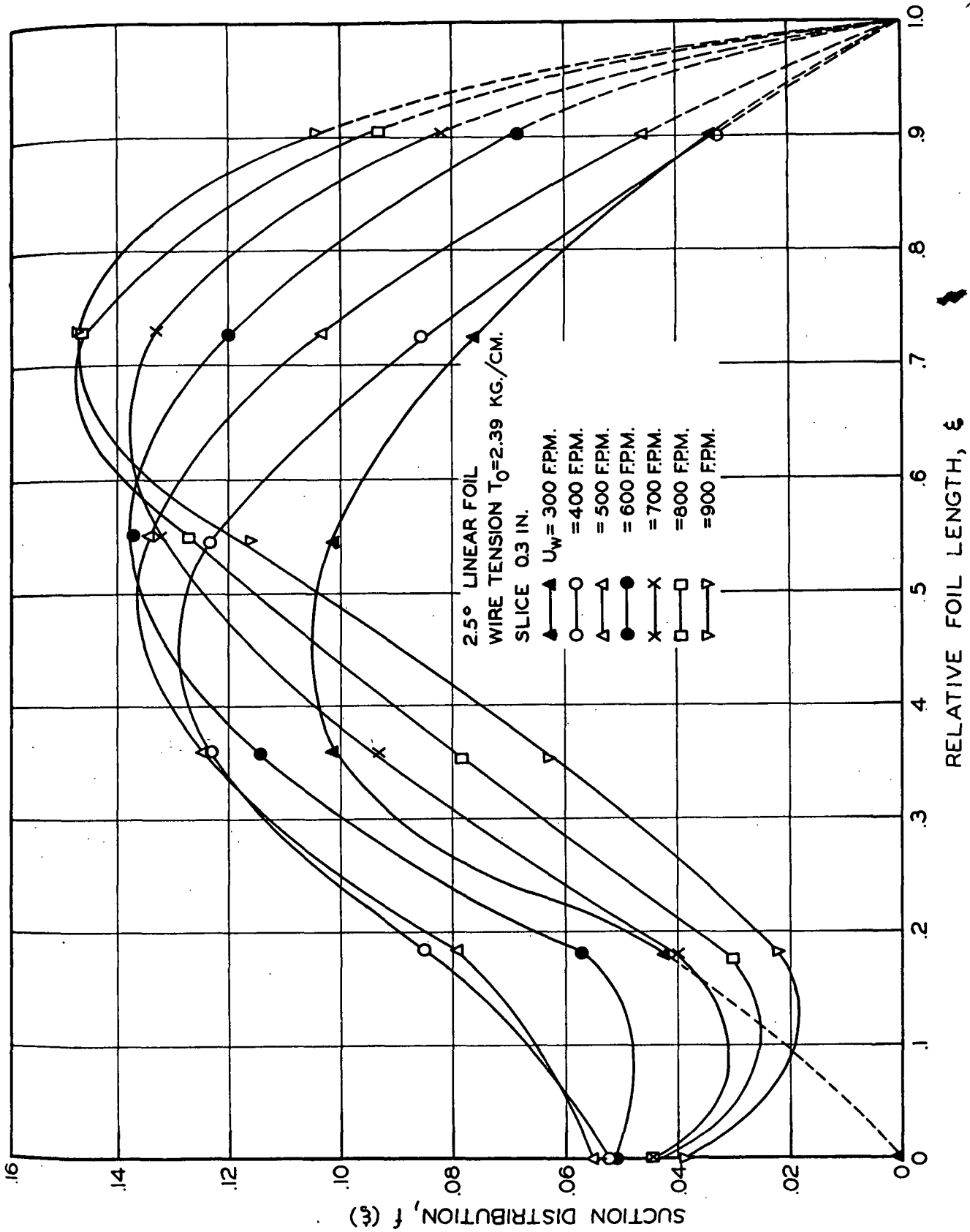


Figure 13. Distribution of Suction at a Foil for Varying Wire Speeds, $\frac{U}{U_w}$

wire speed, as is also reflected in Wrist's foil data (3). With increasing speed, the distributions gradually undergo a significant change: At wire speeds $\underline{U}_w > 700$ f.p.m., all suction maxima are preceded by a minimum occurring close to the point where the wire leaves the support of the foil. It is also worth noticing that suction invariably quits only at the trailing edge of the foils, indicating that the nip is filled with water over its entire length. Maximum suction, as well as the area below the distribution curves, decreases with decreasing wire tension.

The whole variety of profile shapes apparently reflects the effect of subtle changes of the nip geometry which take place along the flexible wire boundary in order to adjust for the varying conditions of equilibrium of the forces involved. In order to aid in the understanding of these phenomena and their effect on drainage, a new attempt to analyze the foil drainage process has been made and is shown in some detail in Appendix I. The results of that analysis in terms of scale factors (i.e., dimensionless groups of the parameters with effect on the flow mechanism of drainage) will be used in order to prepare the data for comparison with predictions.

COMPARISON WITH THEORY

In entering the discussion and interpretation of the corrected foil drainage data as shown in Fig. 9, it seems that the drainage rate, \underline{q}_d , increases with wire speed, \underline{U}_w , angle of inclination, α , and rest wire tension, \underline{T}_0 , in a rather simple manner. Indeed, polynomials could be fitted to each one of the curves with good agreement. But to incorporate in such representation of the data the dependence of drainage on the coefficients \underline{K} and \underline{m} (which were shown earlier to vary with drainage velocity) would be difficult if satisfactory. Such a formulation may be useful for the purpose of numerical interpolation within the given set of data, but could not be used with confidence for extrapolation beyond that range and under no circumstances at all in order to predict drainage under different conditions. It is therefore more profitable to treat the data by the means prepared in the analysis under Appendix I. At first, the experimental data will be evaluated with respect to \underline{K} and \underline{m} . This information then makes their representation in terms of scale factors possible for which, on the other hand, functional relationships are known either in the form of the equations derived or, as in a few cases, as solutions of these equations. In this way, an immediate comparison between experimental and predicted data is possible, indicating the compatibility of the mathematical model and the degree of understanding achieved.

We begin by rewriting the combined formulas (24) and (25) in Appendix I in the form

$$\underline{q}_d = L \left(\frac{\rho U_w^2}{2K} \right)^{1/m} \int_0^1 f(\xi')^{1/m} d\xi' \quad (24a)$$

representing the rate of drainage, \underline{q}_d , and its dependence on the suction distribution, $f(\xi')$, wire speed, \underline{U}_w , length in machine direction of the

linear foil, \underline{L} , and on \underline{K} and \underline{m} , the coefficient and the exponent, respectively, in the drainage law (3). Equation (19) of Appendix I shows that the suction distribution, $f(\xi')$, depends on the wire tension and flow resistance parameters, τ and κ , respectively, and thus, implicitly, on the wire speed, \underline{U}_w , as vividly shown by the suction distribution data, Fig. 10-13. It is, for this reason, not possible to obtain \underline{m} by evaluating the drainage rate data alone, and the following solution method was applied. Equation (24a) may be solved for \underline{K} , resulting in

$$K = 0.5 \left[\frac{L(\rho U_w^2)^{1/m}}{q_d} \int_0^1 f(\xi')^{1/m} d\xi' \right]^m \quad (24b)$$

For each known drainage rate, \underline{q}_d , associated suction distribution, $f(\xi')$, wire speed, \underline{U}_w , and wire tension, \underline{T}_D , this expression may be evaluated for a number of different \underline{m} values in the range $1 \leq \underline{m} \leq 2$, thus yielding a series of $\underline{K}(\underline{m})$ values for each data point. The compatible pair is then obtained by comparing $\underline{K}(\underline{m})$ with the master curve of Fig. 4 by reading off \underline{K} and \underline{m} at the intersection of $\underline{K}(\underline{m})$ with that curve. A sample case for the 4.9° foil at $\underline{U}_w = 700$ f.p.m., rest wire tension, $\underline{T}_D = 1.995$ kg_f/cm., drainage rate, $\underline{q}_d = 1907$ cc./sec./ft. width (from Fig. 9), and the appropriate suction distribution (from Fig. 10) is included in Fig. 4, resulting in $\underline{K} = 0.129$, $\underline{m} = 1.713$. All \underline{m} values found in this way lie within the range of $1.6 < \underline{m} < 1.85$, indicating that superficial flow across the fabric-wire composite is far above the range of Darcy's law (where viscous dissipation of energy dominates the losses) and closer to where effects associated with the wake behind the individual fiber and wire of the porous resistance become all important.

In passing, we may mention that, more often than not, a second intersection with the master curve of Fig. 4 occurs at values of \underline{m} closer to unity.

The decision as to which of the two values is to be used is made on the basis of the associated maximum drainage velocity, v_1 , which can be determined for any related \underline{m} or \underline{K} value by use of Fig. 3. The resulting velocity, v_1 , should be not much smaller than $\alpha U_{\underline{w}}$, an imaginary drainage velocity which would occur if the (linear) foil acted like a retreating piston. It is not too difficult to see that such idealization yields, indeed, an upper-limit estimate of the drainage velocity as long as flow separation from the foil does not occur prematurely and wire tension is sufficiently high.

For all those points which constitute the graph of Fig. 9 and for which the associated suction distributions are known from Fig. 10-13, \underline{K} and \underline{m} values were computed in this way. This, in turn, makes it possible to compute the values of the parameters κ and τ , as defined by Equations (18a) and (18b) of Appendix I for each such experimental point. According to Equations (24) and (25), drainage at a foil should depend on these scale factors together with \underline{m} , rather than on any other combination. The result in terms of relative mean drainage velocity, $\bar{v}/\alpha U_{\underline{w}}$, for the 2.5° and the 4.9° foils is shown in Fig. 14 where the experimental points are plotted as a function of the resistance parameter $1/\kappa$, as suggested by theory. The numbers beside the individual points refer to the reference numbers of Tables I and II where the associated \underline{m} , \underline{K} , and τ values are listed for comparison with those of the solution curves, whose preparation is discussed in Appendix I.

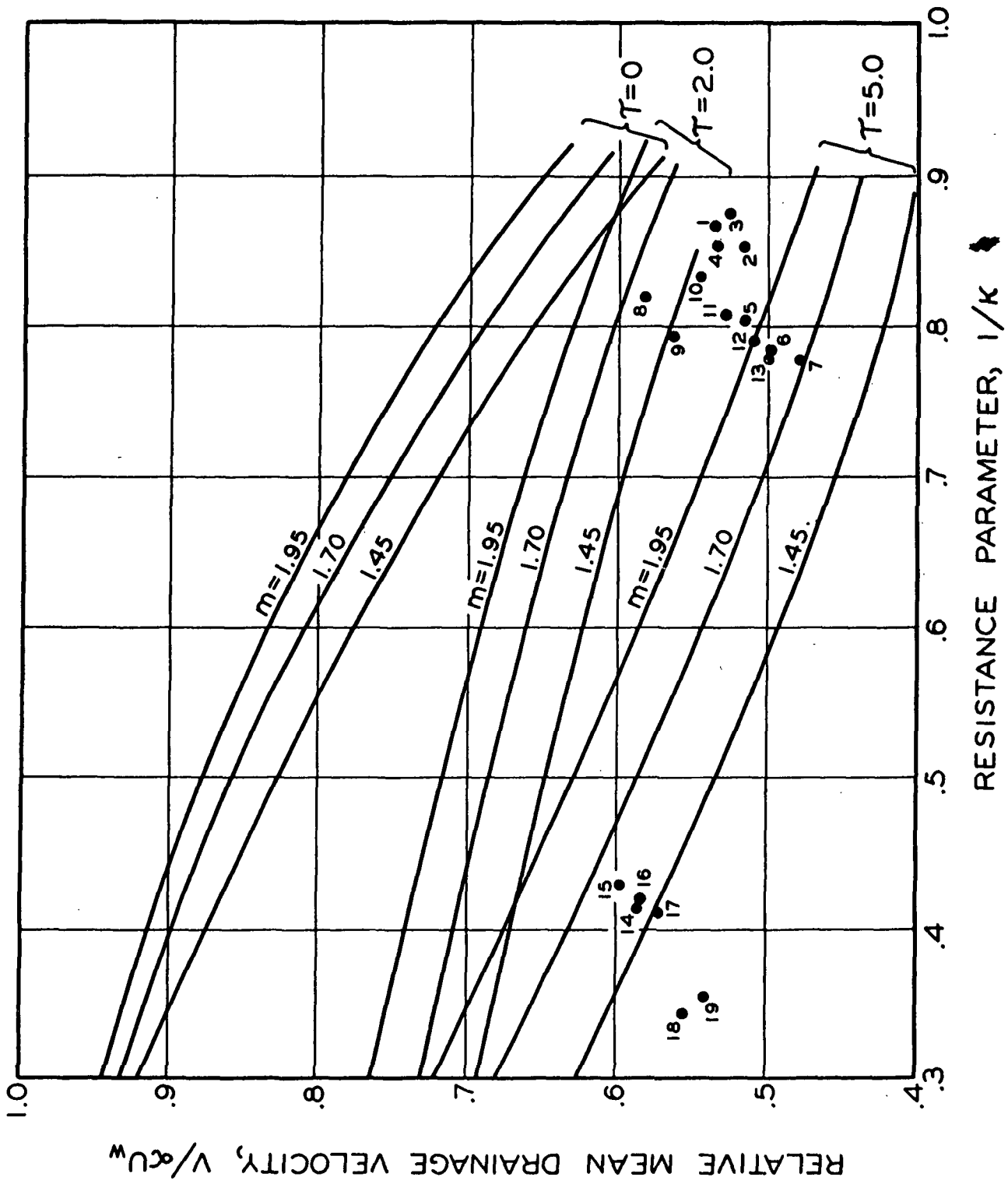


Figure 14. Relative Mean Drainage Velocity as a Function of $1/k$, τ , and m ; Comparison with the Experimental Data

DISCUSSION OF RESULTS

We focus our attention at first on the right-hand cluster of data points of Fig. 14 which all belong to the 4.9° foil. In going from the higher to the lower points one finds by consulting Table I that the accompanying \underline{m} values decrease while the τ values increase, the latter being caused either by increasing wire speed or decreasing wire tension. Considering Fig. 3, a relatively slack wire thus causes the occurring maximum superficial drainage velocity, \underline{v}_1 , to decrease. The fact that in spite of a fairly wide range of actual wire velocities, the abscissa values, $1/\underline{\mu}$, are nearly the same for all points (thus causing the clustering of the points) suggests that, to a certain extent and due to the flexibility of the wire, a self adjustment of drainage is taking place: \underline{K} and \underline{m} vary with increasing wire speed such as to render the resistance parameter (18b) $1/\underline{\mu} \approx (\text{constant}) \alpha$, with the constant having a value of about 10. As may be noticed, the same observations and the same constant of about 10 also hold for the left-hand cluster of points belonging to the 2.5° foil data. For lack of sufficient data for a different fabric-wire system, it may be suggested only as a possibility that the constant varies with the resistance of the porous sheet.

Bearing in mind that experimental errors in collecting the rate and pressure data, the crude assumption made in taking the scraper effect into account, errors in the graphical solution for \underline{K} and \underline{m} , and the fact that the solutions used are of an approximate nature, all contribute to the overall picture given by Fig. 14, the agreement between data and predictions is quite satisfactory. Data and curves demonstrate the large effect of the wire tension parameter, τ , on the mean drainage velocity, $\underline{\bar{v}}$, and that wire tension becomes the more dominating the smaller $1/\underline{\mu}$ (i.e., the smaller either the foil angle, α , or the resistance coefficient, \underline{K} , etc.) happens to be. The figure shows further that, except

perhaps for values of the resistance parameter, $\mu \leq 1$, the theory without the wire tension effect would tend to overpredict drainage to a considerable degree. This observation may explain Taylor's (4) partial success in demonstrating agreement of his prediction with Wrist's data (3).

DEMONSTRATION OF PREDICTION

As limited as the family of solution curves as presented in Fig. 7 may be with respect to the τ values accounted for, this graph can be used for predicting the rate of drainage and immediate comparison with the data of Fig. 9.

In accordance with the parameters of that graph, we assume that the water temperature, the angle of foil inclination, α , the wire speed, \underline{U}_w , the rest wire tension, \underline{T}_0 , and the length of the foil, \underline{L} , is all that is given. The task is to predict drainage, \underline{q}_d , by use of Fig. 14 and 3, the latter representing the indispensable information regarding the flow resistance of wire and mat. The above-given data suffice for computing the numerical value of the wire tension parameter, τ , but the entrance into the graph of Fig. 14 can be gained only by also knowing \underline{K} and \underline{m} . As will be seen from Fig. 3, these coefficients may, depending on the range, \underline{v}_1 , of the drainage velocity, assume an infinite number of values. Therefore, \underline{v}_1 must be known or reasonably estimated. Since the ordinate values of Fig. 14 (representing the ratio of the mean drainage velocity, $\underline{\bar{v}}$, and the "piston" drainage velocity, $\alpha\underline{U}_w$) are always less than unity for finite wire tensions, it follows that $\underline{\bar{v}} < \alpha\underline{U}_w$ but of the same order of magnitude. In view of the meaning of \underline{v}_1 as an upper-limit value of the real drainage velocity, it may be seen that by putting $\underline{v}_1 \approx \alpha\underline{U}_w$ a reasonably acceptable assumption is made. With \underline{v}_1 thus known, the coefficients \underline{K} and \underline{m} may be read from the graph of Fig. 3 and μ computed according to Equation (18b). Upon reading the proper value of $(\underline{\bar{v}}/\alpha\underline{U}_w)$ from Fig. 14 the rate of drainage, \underline{q}_d , is simply computed according to Equation (24), which can be written

$$q_d = \alpha U_w L (\bar{v} / \alpha U_w) \quad (24b)$$

A number of points suitable for convenient interpolation with respect to the parameters τ and \underline{m} of Fig. 14 have been computed according to the following table (Table III) and entered into Fig. 9 for comparison with the data curves. Most of the computed points overpredict drainage by not more than 15%, as compared with as much as 55% if the ideal ($\tau = 0$) theory were used for predicting drainage at the 2.5° foil.

TABLE III
PREDICTION OF FOIL DRAINAGE

α	T_0	U_w	τ	$v_1 \approx \alpha U_w$	K	m	$1/\mu$	$\bar{v}/\alpha U_w$	$(q_d)_{pred.}$	$(q_d)_{pred.}/(q_d)_{meas.}$
$^\circ$	kg _f /cm.	f.p.m.	cm./sec.	(^a)	(^a)	(^b)	cc./sec.cm. /ft. width			
4.9	0.855	500	1.8	21.7	0.25	1.494	0.851	0.56	1445	1.085
4.9	0.855	700	3.54	30.45	0.197	1.583	0.79	0.51	1840	1.10
4.9	1.5	700	2.01	30.45	0.197	1.583	0.79	0.58	2090	1.16
4.9	1.5	900	3.33	39.10	0.163	1.644	0.75	0.53	2460	1.14
2.5	1.62	500	1.9	11.1	0.363	1.325	0.347	0.68	903	1.21
2.5	2.39	700	2.5	15.5	0.320	1.405	0.36	0.66	1215	1.14
2.5	2.39	900	4.13	19.9	0.264	1.475	0.344	0.60	1430	1.16

^a From Fig. 3.

^b From Fig. 14.

CONCLUSIONS

The quantitative agreement between converted experimental data and predictions according to Fig. 14 leaves something to be desired; however, it is questionable whether a better agreement can be expected, as may be appreciated from the following remarks:

1. The approximate solution (30) used in drawing the two families of curves for $\tau = 2$ and 5 satisfies the boundary condition of zero suction at the trailing edge of the foil and the differential-integral equation (19) with respect to the initial and maximum values of suction, but it is not the true solution of that equation and for that reason does not exhaust the power of the mathematical model. [Equations (11-30), Appendix I.]

2. The converted data contain the cumulative effect of errors in the rate and suction measurements in the graphical solution for \underline{K} and \underline{m} . Also, the crude assumption of constant \underline{K} and \underline{m} in accounting for the effect of the scraper necessarily introduces a source of error. A separate investigation is presently in progress to examine and measure this effect more precisely.

3. Although the present nonviscous theory predicts suction in the correct magnitude, viscosity may also have some effect, particularly for small foil angles and/or low wire tensions. However, the present precision of the converted data is not high enough to make such effects recognizable.

4. Suction distribution and drainage depend apparently on the stiffness or rigidity of the wire, as shown by comparing the nonrigid (slack-fabric) model applied in the analysis with the real wire (as far as it can be inferred from the shape of the measured suction profiles at the higher wire speeds). It appears that the inclusion of wire stiffness would have its greatest effect in the range

of the smaller $1/\mu$ and/or α values. In this connection, it could be suggested that spouting behind drainage elements may be associated with wire rigidity because the latter affects the geometry of the wire boundary.

5. In the approximate analysis of wire tension under operational conditions only the effect of centrifugal forces was numerically estimated and found negligible. It is possible that the contribution of wire deflection is greater than was here assumed for convenience, in which case most of the τ values of the data points would be somewhat too high.

Aside from the quantitative aspects of the comparison, Fig. 14 and Tables I and II show that there is good qualitative agreement between data and analysis, suggesting proof of the following:

1. Wire tension [or rather, wire tension parameter τ as defined in (18a)] and drainage resistance [or rather, drainage resistance parameter μ as defined in (18b)] control and determine the mean drainage velocity \bar{v} through the sheet, and consequently, drainage itself. A further parameter of significance (but not varied in this investigation) is the relative distance between consecutive foils, λ . Slackening of the wire (as expressed by increasing τ) reduces drainage at large-angle foils relatively more than at a foil with small angle, α .

2. As long as the wire deflection can be modeled as a fabric of zero stiffness, maximum suction at a linear foil could be shown [by utilizing Equations (21), (18b), and (18c)] to become

$$P_{\max} = (\alpha U_w)^m K \left\{ 1 - \tau \left[g'(1) - g'(\xi_1) + \lambda (g(1) - g'(1)) \right] \right\}^m,$$

which is always smaller than $\rho U_w^2 / 2$, as would occur at a table roll under ideal

flow conditions and for $\tau = 0$ (infinite wire tension). As may be seen, maximum suction can be varied by varying the wire tension; its amount also depends directly on the m th power of the "piston" velocity, αU_w .

3. Both analysis and data show that suction sets in with a finite value instead of gradually increasing from zero; likewise, the initial suction decreases with a lowering of the wire tension. The first-mentioned observation can be made wherever flow follows around a corner by forming a wall jet, a phenomenon sometimes referred to as Coanda effect (5). It could be shown that wherever foil suction is finite, the associated nip flow includes layers with velocities greater than the wire speed, a situation analogous to that in a wall jet.

Upon improving our understanding of the scraper effect, the present data will be re-evaluated and the result communicated. In the course of this part of the work, the graph of Fig. 14 will be extended to include curves for additional values of the wire tension parameter, τ , in order to facilitate interpolation for prediction purposes.

In conclusion, it appears that the predictability of foil drainage has been extended to more realistic conditions and improved by including a more general drainage law and the effect of wire tension in the analysis.

Although it would involve additional difficulties, a more sophisticated wire model (e.g., the one discussed in Appendix II) could be incorporated in order to study its effect on deflection, suction distribution, and subsequent spouting.

The step from drainage at an individual foil to the drainage profile along a series of foils and under the increasing flow resistance of a growing mat will be relatively simple, but it would be premature to do it at this time and state of affairs.

ACKNOWLEDGMENTS

The authors wish to express their appreciation to Mr. O. C. Kuehl whose skill and help in expanding the hydraulic system, in constructing the new flow spreader, and in the performance of the experiments made this investigation possible. Acknowledgment is also made to Messrs. Harold Grady and Lester Nett for their help in conducting the experiments. Our thanks also go to Mrs. Elizabeth Cary for expertly pre-editing and typing this report.

NOMENCLATURE

- \underline{a}' = viscous resistance, l/cm.
 \underline{a}_b = $\mu \underline{a}'$
 $\underline{a}_1, \underline{a}_2$ = coefficients defined by Equation (30)
 \underline{b}' = inertial resistance, dimensionless
 \underline{b}_b = $\rho \underline{b}'$
 \underline{c} = exponent, dimensionless
 \underline{D}_α = drag force on foil, g. force/cm.
 \underline{E} = modulus of elasticity, g. force/cm.²
 $\underline{f}_1(\underline{K}),$
 $\underline{f}_2(\underline{K}),$
 $\underline{F}(\underline{K})$ = functions associated with boundary layer theory
 $\underline{f}(\underline{\xi})$ = suction distribution function, dimensionless
 \underline{f} = boundary layer friction factor, dimensionless
 $\underline{F}(\underline{x})$ = linear load on wire segment, g. force/cm.
 $\underline{g}(\underline{\xi})$ = suction load distribution function, dimensionless
 $\underline{h}(\underline{x})$ = local wire deflection, cm.
 \underline{h}_b = initial thickness of water layer above porous sheet, cm.
 \underline{I} = moment of inertia, cm.⁴

- \underline{K} = drainage coefficient in power law; shape factor in boundary layer theory, dimensionless
- \underline{L} = length of foil in machine direction, cm.
- $\underline{L}_1, \underline{L}_2$ = lengths in machine direction of unsupported wire screen, cm.
- \underline{m} = exponent in power law, dimensionless
- $\underline{M}(x)$ = bonding moment, g. cm.
- \underline{n}_f = number of pairs of foils, dimensionless
- \underline{p} = local suction, g. force/cm.²
- $\underline{P}(\xi)$ = defined by Equation (20)
- \underline{q} = predicted drainage rate, cc./sec. cm.
- \underline{q}_t = total drainage rate at matching jet and wire speed, cc./sec. cm.
- \underline{q}_d = drainage rate due to hydrodynamic action, cc./sec. cm.
- \underline{q}_{bg} = drainage rate due to gravitation, cc./sec. cm.
- \underline{q}_{s} = rate of backwash at a scraper, cm.²/sec.
- \underline{R} = radius of roll, cm.
- \underline{s} = slice opening, cm.
- \underline{S} = overall length of deflected wire screen, cm.
- \underline{T} = horizontal component of wire tension, g. force/cm.
- \underline{T}_0 = rest wire tension, g. force/cm.
- \underline{u} = velocity component, cm./sec.
- \underline{U}_j = fully developed slice jet velocity, cm./sec.
- \underline{U}_w = wire or machine speed, cm./sec.
- \underline{v} = superficial velocity component in y-direction, cm./sec.
- $\underline{\bar{v}}$ = mean drainage velocity, cm./sec.
- \underline{v}_1 = maximum drainage velocity, cm./sec.
- \underline{v}_{opt} = drainage velocity associated with ideal table roll drainage, cm./sec.
- \underline{V} = vertical component of wire tension, g. force/cm.

- $\underline{x}, \underline{x}'$ = coordinates
- \underline{y} = coordinate
- \underline{y}_0 = thickness of water layer hanging under the wire, cm.
- α = angle of inclination of linear foil, rad.
- γ = scraper angle of attack, rad.
- δ = thickness of wire screen, cm.
- δ^* = displacement thickness, cm.
- $\Delta \underline{P}$ = overall pressure drop, dynes/cm.²
- $\Delta \underline{T}_{\underline{c}}, \Delta \underline{T}_{\underline{w}}$ = increase of wire tension due to centrifugal forces and wire wrap,
g. force/cm.
- ϵ = porosity, dimensionless
- θ = momentum thickness, cm.
- κ = drainage resistance parameter defined by Equation (18b)
- λ = relative foil separation defined by Equation (18d)
- μ = viscosity of water, g. force sec./cm.²
- ν = μ/ρ = kinematic viscosity of water, cm.²/sec.
- ξ, ξ' = nondimensional nip coordinates
- ξ_1 = position of suction maximum
- ρ = mass per unit volume of water, g. mass/cm.³
- $\rho_{\underline{w}}$ = mass of wire screen material, g. mass/cm.³
- σ = defined in Equation (55)
- τ = wire tension parameter, defined by Equation (18a)
- τ_0 = wall shear stress, g. force/cm.²
- τ_1 = defined by Equation (18c)
- φ = distribution constant, dimensionless
- Φ = defined by Equation (7), dimensionless

LITERATURE CITED

1. Meyer, H. Hydrodynamic drainage through sheets of constant resistance. I. Preliminary results for a 2-in. diameter table roll. Report Four, Project 2570. Appleton, Wis., The Institute of Paper Chemistry, May 17, 1967.
2. Andrews, B. D. Construction of a device for studying drainage at rolls and foils. Report Three, Project 2570. Appleton, Wis., The Institute of Paper Chemistry, May 11, 1967.
3. Burkhard, G., and Wrist, P. E., Pulp Paper Mag. Can. 57:100(1956).
4. Taylor, G. I., Pulp Paper Mag. Can. 59, Conv. Issue:172(1958)
5. Wille, R., and Fernholz, H., J. Fluid Mech. 23:801(1965).
6. Taylor, G. I., Pulp Paper Mag. Can. 57, Conv. Issue:267(1956).
7. Bergstroem, J., Svensk Papperstid. 60, no. 1:1(1957).
8. Meyer, H., Tappi 47, no. 2:114(1964).
9. Schlichting, H. Boundary layer theory. New York, McGraw-Hill, 1960.

THE INSTITUTE OF PAPER CHEMISTRY

H. Meyer

H. Meyer, Research Associate
Mechanical Processes Group
Technology Section

B. D. Andrews

B. D. Andrews, Research Fellow
Mechanical Processes Group
Technology Section

APPENDIX I

DRAINAGE AT A FOIL

A theory of drainage at a foil is available from a paper by Sir G. I. Taylor (4). On the ground that "the effect of turbulence on the distribution of suction in the table roll problem" was found "not so great as to make the solution of the idealized problem of drainage at a foil useless," the problem was dealt with under the assumption that perfect (turbulent) mixing would render the distribution of velocity in the nip uniform. But measurements (3) of suction at table rolls do not suggest that peak suction comes even only near the amount of $1.4\rho U_w^2/2$ postulated by Taylor's perfect mixing model. Rather, they are in apparent favor of Taylor's streamline model which predicts a maximum suction of $\rho U_w^2/2$.

It was realized at a fairly early stage of this investigation that our data could be satisfactorily interpreted only if a drainage law more general than Darcy's and the effect of finite wire tension were taken into account. Inclusion of these effects makes Taylor's momentum balance approach again intractable, i.e., requiring numerical solution of the resulting differential-integral equation. For this reason, and also in the interest of a unified approach to all conventional paper machine drainage problems, the streamline model of flow in the nip between foil and wire was adopted in the following analysis.

When the relationship between the superficial velocity, v , of flow across the porous composite and suction, p , is assumed to be of the form shown in Equation (3), the assumption of streamline flow in the nip of a linear foil of length L set at a small inclination, α , to the horizontal and below a wire moving at speed U_w leads to the following description of suction:

$$\frac{\alpha x}{L} - \frac{h(x)}{L} = \left[\frac{(\rho U_w^{2-m}/2K)^{1-m}}{L} \right] \int_0^x f(x')^{1/m} [1 + f(x) - f(x')]^{-1/2} dx' \quad (11)$$

where $f(\underline{x})$ is the suction distribution defined by

$$f(x) = 2p(x)/\rho U_w^2 \quad (12)$$

The dummy variable \underline{x}' varies between 0 and \underline{x} . $\underline{h}(\underline{x})$ is the deflection of the wire under the prevailing suction load. Figure 15 defines the coordinate system used and shows the geometric situation for two consecutive foils as assumed in the analysis. The deflection, $\underline{h}(\underline{x})$, of a wire screen whose resistance to deformation stems solely from tension rather than rigidity may be described in terms of the following familiar equation:

$$d^2 h/dx^2 = - \frac{\rho U_w^2}{2T} f(x) \quad (13)$$

where T is the wire tension in terms of force per unit width of wire and where it was assumed that the contribution of the centrifugal force to the deflecting load is negligible. Upon integrating and satisfying the conditions $\underline{h}(0) = \underline{h}(L_1) = 0$, the wire deflection is obtained as

$$h(x) = \frac{\rho U_w^2}{2T} \left\{ \left[\int_0^L \int_0^L f dx dx + (L_1 - L) \int_0^{L_1} f dx \right] \frac{x}{L_1} - \int_0^x \int_0^x f dx dx \right\} \quad (14)$$

Upon introducing the nondimensional nip length variable,

$$\xi = x/L \quad (15)$$

into Equations (11) and (14), the following equation results:

$$(1 - \tau_1)\xi + \tau g(\xi) = \int_0^\xi f(\xi')^{1/m} [1 + f(\xi) - f(\xi')]^{-1/2} d\xi' \quad (16)$$

where

$$g(\xi) = \int_0^{\xi} \int_0^{\xi'} f(\xi') d\xi' d\xi \quad (17)$$

and where:

$$\text{wire tension parameter: } \tau = \rho U_w^2 L / 2\alpha T \quad (18a),$$

$$\text{drainage resistance parameter: } \kappa = (\rho U_w^2 / 2K)^{1/m} / \alpha U_w = v_{opt} / \alpha U_w \quad (18b),$$

$$\tau_1 = \tau [\lambda g(1) + (1 - \lambda) g'(1)] \quad (18c),$$

$$\text{relative foil separation: } \lambda = L / L_1 \quad (18d).$$

The drainage resistance parameter, κ , may be interpreted as the ratio of "piston" velocity, αU_w , and optimal drainage velocity, v_{opt} , which would occur if the maximum suction, \underline{p} , were equal to that at a table roll, where under ideal conditions $\underline{p}_{max} = \rho U_w^2 / 2$. The boundary condition on $f(\xi)$ is $f(1) = 0$, which assures that the suction at the foil trailing edge vanishes. The integral Equation (16) transforms, upon differentiating, into the differential-integral equation

$$[(1 - \tau_1)\xi + \tau g(\xi) - \kappa P(\xi)] f'(\xi) - 2\kappa f(\xi)^{1/m} + 2[1 - \tau_1 + \tau g'(\xi)] = 0 \quad (19)$$

with

$$P(\xi) = \int_0^{\xi} f(\xi')^{1/m} [f(\xi) - f(\xi')] [1 + f(\xi) - f(\xi')]^{-3/2} d\xi' \quad (20).$$

Certain useful conclusions can be drawn from these equations. Whenever suction reaches a maximum, one has $f' = 0$ and Equation (19) gives

$$f(\xi_1) = \left[\frac{1 - \tau_1 + \tau g'(\xi_1)}{\kappa} \right]^m \quad (21)$$

as the amount of maximum suction occurring at the point ξ_1 somewhere along the foil. As Equation (21) shows, maximum suction is reduced at finite wire tensions where $\tau \neq 0$.

Writing Equation (16) for the foil's trailing edge where $\xi = 1$ and $f(1) = 0$, the expression

$$1 - \tau_1 + \tau g(1) = \lambda \int_0^1 f(\xi')^{1/m} [1 - f(\xi')]^{-1/2} d\xi' \quad (22)$$

is obtained. In order for the integrands of Equations (20) and (22) to remain real when passing through the point $\xi' = \xi_1$, it is necessary that $f(\xi_1) < 1$, thus limiting peak suction to values $p(\xi_1) \leq \rho U_w^2 / 2$. In view of Equation (21), peak suction may be expected to depend on the numerical values of the parameters τ , κ , and λ , rather than to assume a universally constant value (e.g., the value of unity for the table roll problem in the absence of wire wrap).

The rate of flow discharging from the end cross section of the nip may be called drainage, q_d . When nip flow does not separate from the inclined foil surface, the volume rate of drainage is obtained by integrating the rate of permeation flow through the wire over the entire length, L , of the foil,

$$q_d = \int_0^L v dx \quad (23)$$

Employing Equations (3) and (12), drainage can then be expressed in terms of the suction distribution function, $f(\xi)$, in a number of ways as follows:

$$q_d = \begin{cases} L\bar{v} \\ L \left(\frac{\rho U_w^2}{2K} \right)^{1/m} Q(\tau, \kappa, \lambda) \\ \alpha L U_w \kappa Q(\tau, \kappa, \lambda) \end{cases} \quad (24)$$

where

$$Q = \int_0^1 f(\xi')^{1/m} d\xi' \quad (25)$$

and where \bar{v} is the mean drainage velocity through the porous sheet. Since $f(\xi')$, as a solution of Equation (19), depends on the nondimensional parameters τ , λ , and κ , drainage, q_d , is subjected to the same parameters. Equation (24) may be looked at as the result of a dimensional analysis of drainage at a linear foil under the assumption that the drained fluid is an ideal (nonviscous) fluid. The scale factors thus obtained may be useful in presenting experimental data for comparison with predictions.

The law of interaction of these scale factors and their effect on drainage could be found by generating solutions of either one of Equations (16) or (19) under numerical variation of the parameters. Quite obviously, finite wire tension, \underline{T} , (and therefore, nonzero τ 's--complicate the above equations and intermediate results considerably. In order to gain some familiarity with the problem, Equation (19) was first solved for $\tau = \tau_1 = 0$. It reduces in such case to

$$[\xi - \kappa P(\xi)]f'(\xi) - 2\kappa f(\xi)^{1/m} + 2 = 0 \quad (26)$$

with $\underline{P}(\xi)$ as defined by Equation (20) and the boundary condition $f(1) = 0$.

The numerical solution of the differential-integral equation [Equation (26)] proceeds from an approximate first to the final solution through a converging sequence of successive approximations and need not be represented here in detail.

A sample graphical representation of the suction distribution function, $f(\xi)$, for $m = 1.0$ and a number of κ values between $1/0.9$ and 5.0 is shown in Fig. 16. The dependence of the drainage factor, Q , on the resistance parameter $1/\kappa$ and the exponent m of the law (3) is shown in Fig. 17. The suction distribution curves of Fig. 16 are very close to Taylor's (4) in the range of his a values smaller than 0.5 , and obtained by way of an entirely different approach. As is apparent from Fig. 17, the relationship between Q and its constituent is not a simple one. For small values of κ , the following formula gives values which are in good agreement with those of Fig. 17,

$$Q \approx \frac{2(1/\kappa)}{2 + m(1/\kappa)^m} \quad (27)$$

where $1/\kappa$ corresponds to the abscissa values of that figure. Replacing the drainage factor, Q , in Equation (24) by the above expression gives

$$q_d \approx \alpha L U_w \frac{2}{2 + m(1/\kappa)^m} \quad (\tau = 0) \quad (28)$$

which should predict drainage well for $\tau = 0$ and small values of $1/\kappa$. Equation (28) completes this part of the analysis.

To prepare a similar equation for the practically more important case of finite wire tension is the purpose of solving Equation (19) for τ and $\tau_1 \neq 0$.

When $\xi = 0$, which is the point where the wire leaves the foil, Equation (19) could be shown to yield as the starting value of suction

$$f(0) = \left(\frac{1 - \tau_1}{\kappa} \right)^m \quad (29)$$

where, by (18c), τ_1 depends on $g(1)$ and $g'(1)$ and, because of (17), on the

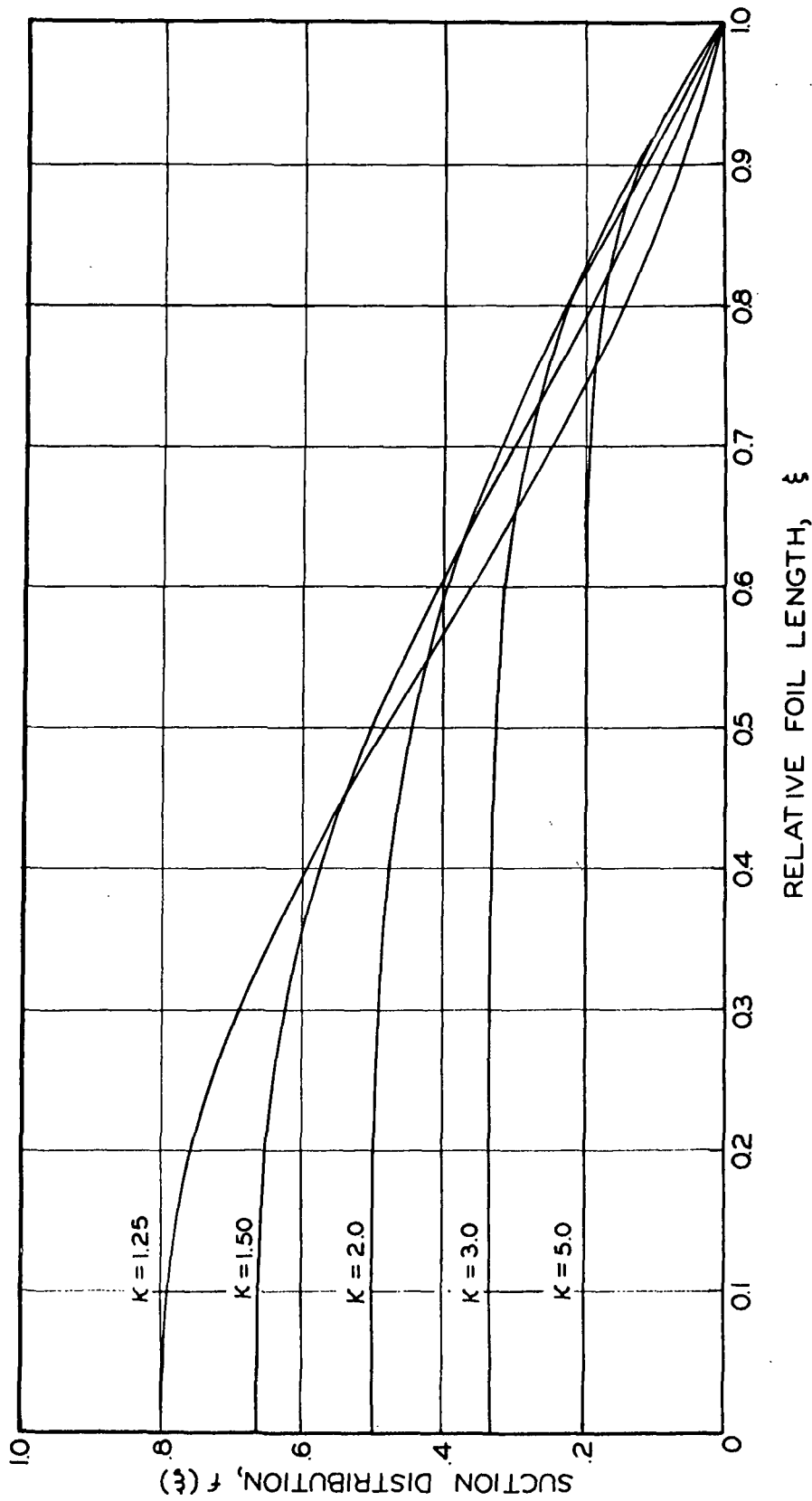


Figure 16. Distribution of Suction at a Plane Foil with Tangent Wire for $m = 1.0$ ($\tau = 0$)

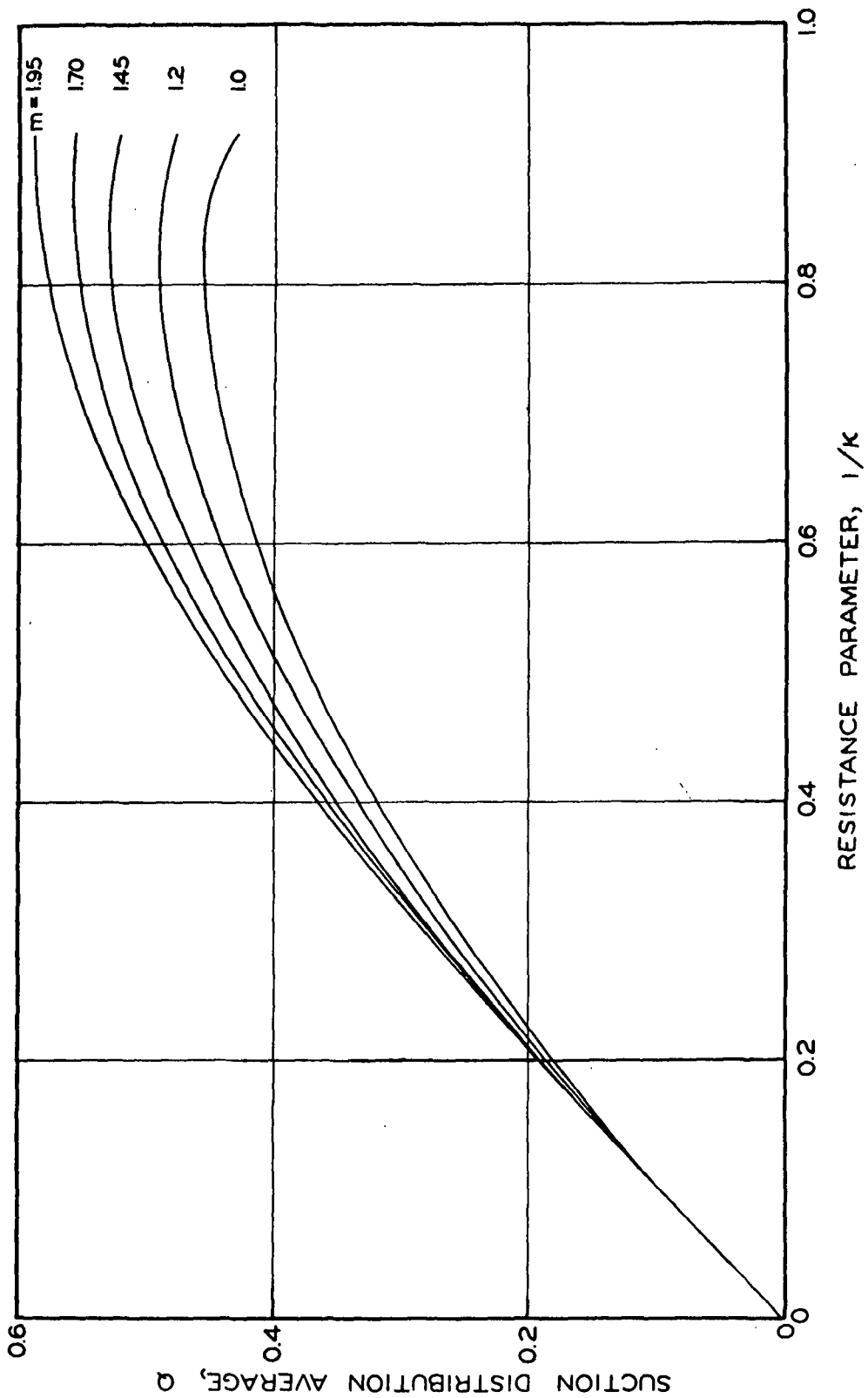


Figure 17. Suction Distribution Average, Q , Versus Resistance Parameter

solution sought. This is also true of the optimum suction given by Equation (21) which in the present case turns out to be a maximum. For a starting approximation of the suction distribution, a second-degree polynomial,

$$f(\xi) = f(0) + a_1\xi + a_2\xi^2 \quad (30),$$

was assumed and the coefficients a_1 and a_2 determined from the boundary condition $f(1) = 0$ and the initial and maximum suction as given by Equations (29) and (21), respectively. Three transcendental equations for $f(0)$, $f(\xi_1)$, and ξ_1 result, which were solved numerically for a number of values of the parameters τ , κ , λ , and m . From here, successive approximations would again lead to converging solutions of Equation (19). A more detailed representation of the entire solution method will be given elsewhere.

It could be shown that both the approximate suction distribution according to Equation (30) and final solutions to Equation (19) are capable of generating all essential features of the measured suction distributions according to Fig. 10 to 13 with one important exception, however: Due to the choice made regarding the mechanical model of the deflecting wire screen by adopting Equation (13), the solutions are incapable of describing the initial sagging of the suction distributions at the higher wire speeds. For the case where this detail becomes important enough to be included in future analyses, a higher order mechanical model of the wire is suggested in Appendix II, which takes care of this flaw.

With the coefficients of the approximate solution (30) known, functional values of the nondimensional drainage coefficient

$$n_d = \bar{v}/\alpha U_w$$

as defined by Equation (24) can be computed, which lends itself to immediate

comparison with experimental data. Figure 14 shows three sets of curves, each computed by choosing $\underline{m} = 1.45$, 1.7 , and 1.95 . The upper set is representative of the ideal case of a tangent wire at $\underline{T}_0 \rightarrow \infty$ and $\tau = 0$, i.e., by use of the solution \underline{Q} as shown in Fig. 17. The two lower sets were computed for two finite values of the wire tension parameter $\tau = 2.0$ and 5.0 by use of the approximate solutions associated with Equation (30).

APPENDIX II

DEFLECTION OF A RIGID WIRE UNDER TENSION

A comparison of the measured suction profiles, Fig. 10-13, with the predicted suction distributions of Equations (16) and (17) shows that the peculiar initial increase of pressure (decrease of suction) observed at the higher wire speeds is not contained in the theory. It appears this is due to the convenient assumption made by adopting Equation (13), i.e., that the wire screen would deform like a fabric of zero rigidity or stiffness. The data suggest a wire-foil nip as in Fig. 18 such that an initial divergence is followed by a temporary convergence, after which the contours of foil and wire would again diverge. Since real wire screens have a certain stiffness which prevents them from deforming with a break (as the fabric model does at the nip origin), a finite rigidity will be assumed in the following analysis. In setting the conditions under which the screen element of Fig. 19 is in mechanical equilibrium, a moment, $\underline{M(x)}$, resisting bending must be taken into account.

Equilibrium with regard to translations in the \underline{x} and \underline{y} directions and with regard to rotation requires

$$\frac{dT}{dx} = 0 ; \quad \text{i.e., } T = \text{constant} \quad (31) ,$$

$$\frac{dV}{dx} = -F(x) \quad (32) ,$$

$$V + \frac{dM}{dx} - T \frac{dy}{dx} = 0 \quad (33) .$$

Eliminating the tension component, \underline{V} , between the last two equations yields

$$T \frac{d^2y}{dx^2} = \frac{d^2M}{dx^2} - F(x) \quad (34) .$$

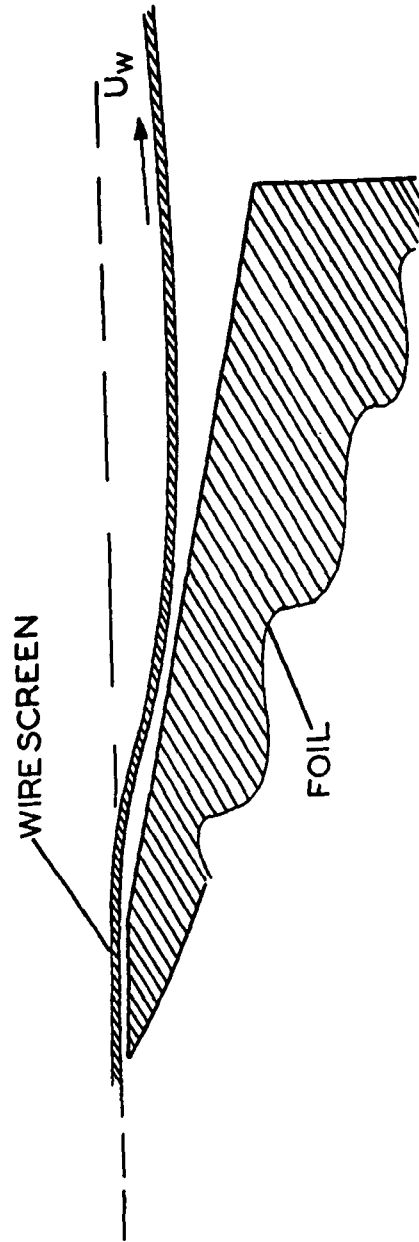


Figure 18. Suggested Form of the Drainage Nip for a Stiff Wire Under Load

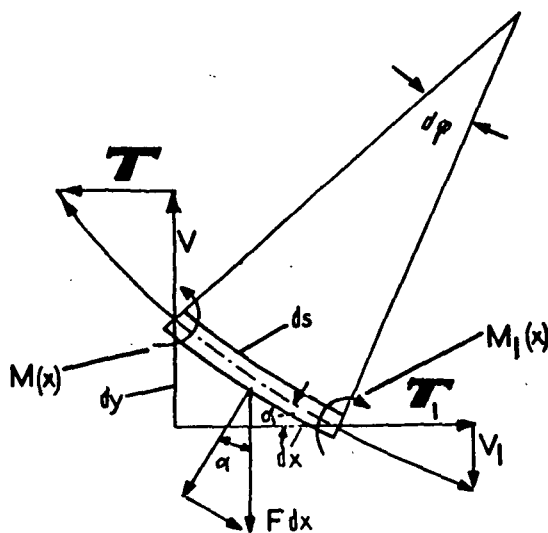


Figure 19. Equilibrium of a Stiff Wire Element Under a Tension, T , and Linear Load, F

The moment M represents the elastic resistance of the wire to bending which may be assumed to increase with decreasing radius of bending. For small deformations we put

$$M(x) = EI \frac{d^2 y}{dx^2} \quad (35)$$

with EI as the rigidity of the wire. When the vertical load, $F(x)$, stems from the suction loading, $p(x)$, only, then for small wire deflections

$$F(x) = \sqrt{1 + y'^2} p(x) \approx p(x) \quad (36)$$

Introduction of the last two equations into Equation (34) results in the fourth-order equation

$$EIy^{IV} - Ty'' - p(x) = 0 \quad (37),$$

which, for a fabric of negligible modulus of elasticity, $E \approx 0$, reduces to Equation (13). In addition to the necessary boundary conditions $y(0) = y(L_2) = 0$ (satisfied also in the slack fabric-wire model), finite values for the initial slope, $y'(0)$, and the end slope, $y'(L_2)$, can now be prescribed. For convenience, $y'(0) = y'(L_2) = 0$ may be chosen.

A solution of Equation (37) satisfying these boundary conditions was prepared and could be used instead of the slack fabric solution (14) if need arises. The resulting integral-differential equation is considerably lengthier than (16), but it could be also brought to a numerical solution.

APPENDIX III

ESTIMATE OF EFFECT OF FRICTION AND DISPLACEMENT THICKNESS

Whereas one might argue that for a number of good reasons the effect of viscosity on table-roll nip flow is not too critical, the same cannot be said a priori of the foil nip flow. There, the surface of the foil is stationary and consequently gives rise to large velocity gradients in its vicinity with two possible effects on drainage:

1. The total mechanical energy available for drainage is reduced by the amount of frictional losses, primarily in the foil boundary layer.
2. The nip cross section available to the flow of drained fluid is reduced by the displacement thickness, primarily of the foil boundary layer, as compared to the geometric cross section available to an ideal fluid.

The magnitude of both effects may be roughly estimated for a single case by making a few computations for a boundary layer as it would develop under the pressure distribution of the ideal fluid theory of Appendix I.

Following Holstein and Bohlen's method as represented in Schlichting's book (9), the displacement thickness, δ^* , and the wall shear stress, τ_0 , can be obtained by use of the relationships

$$\frac{\tau_0 \theta}{\mu u(x)} = f_2(K) \quad (38)$$

$$\frac{\delta^*}{\theta} = f_1(K) \quad (39)$$

where the momentum thickness, θ , is a solution to the equation

$$\frac{d}{dx}(\theta^2/v) = \frac{F(K)}{\mu(x)} \quad (40),$$

and where the shape factor, K , is a given function of $\Lambda = (dp/dx)[\delta^2/\mu u(x)]$, with $u(x)$ being the velocity outside the boundary layer of local thickness $\delta(x)$.

It could be shown that the fluid velocity, $u(\xi)$, along the foil's inclined surface in terms of wire speed, U_w , and suction distribution, $f(\xi)$, is given approximately by

$$u(\xi) = U_w \sqrt{1 + f(\xi)} \quad (41),$$

while the pressure gradient is

$$\frac{-dp}{dx} = \frac{\rho}{2} \frac{U_w^2}{L} f'(\xi) \quad (42).$$

Our estimate will be made for the case of a horizontal wire for which $\tau = \tau_1 = 0$, and with a κ value of 5.0, which causes (as shown in Fig. 16) a constant suction, $f(\xi) = \bar{f}$ and $f'(\xi) = 0$, over most of the length of the foil. Then $\Lambda = 0$, and Equation (40) can be integrated to yield

$$\theta = 0.686 \sqrt{\frac{xv}{U_w \sqrt{1 + \bar{f}}}} \quad (43)$$

so that by (38) and (39),

$$\delta^* = 1.752 \sqrt{\frac{vx}{U_w \sqrt{1 + \bar{f}}}} \quad (44)$$

and

$$\tau_0 = 0.346 \rho U_w^2 (1 + \bar{f})^{3/4} \sqrt{\frac{v}{U_w x}} \quad (45),$$

respectively, result. With the exception of the factors involving $(1 + \underline{f})$, these formulas are identical with those obtained for the flat plate. The displacement thickness, δ^* , may be compared to the width of the nip, $\alpha \underline{x}$, by computing the ratio

$$\frac{\delta^*}{\alpha \underline{x}} = \frac{1.752}{\alpha} \sqrt{\frac{\nu}{U_w \sqrt{1 + \underline{f}} \underline{x}}} \quad (46)$$

For a foil of length $\underline{x} = \underline{L} = 1.5$ in. and angle $\alpha = 0.0436$ rad. ($= 2.5^\circ$), wire speed $\underline{U}_w = 2000$ f.p.m., water at 68°F ., and a relative suction $\underline{f} = 0.2$, this ratio becomes $(\delta^*/\alpha \underline{x})_{\underline{L}} = 6.52\%$ at the end of the foil and $(\delta^*/\alpha \underline{x})_{\underline{L}/2} = 9.25\%$ at its midpoint.

The foil drag force, \underline{D}_α , per unit width can be computed from

$$\underline{D}_\alpha = \int_0^{\underline{x}} \tau_0 dx \quad (47)$$

The equivalence of this force is a pressure force, $\Delta \underline{p} \alpha \underline{x}$, where $\Delta \underline{p}$ is the necessary pressure difference. Consequently,

$$\Delta \underline{p} = \frac{1}{\alpha \underline{x}} \int_0^{\underline{x}} \tau_0 dx \quad (48)$$

represents the approximate amount of pressure by which the suction produced by an ideal fluid will be reduced due to skin friction at the foil. By executing the integration with τ_0 from Equation (45), one obtains

$$\frac{\Delta \underline{f}}{\underline{f}} = \frac{2 \Delta \underline{p}}{\rho U_w^2 \underline{f}} = 1.384 \frac{(1 + \underline{f})^{3/4}}{\sqrt{\frac{\nu}{U_w \underline{x}}}} \quad (49)$$

When the data of the abovementioned example are introduced into the last relationship, one gets $(\Delta \underline{f}/\underline{f})_{\underline{L}/2} = 41.8\%$ at the foil's midpoint and $(\Delta \underline{f}/\underline{f})_{\underline{L}} = 29.4\%$ at

its end. These numbers serve to indicate that frictional effects may indeed have a significant effect on suction, but they should not be taken too seriously as far as their magnitude is concerned for the following main reasons: Boundary layer theory is valid only some distance away from the beginning of the boundary layer in whose vicinity certain assumptions do not hold true. One must further bear in mind that in view of the crosswise dimension of the nip, flow inside and flow outside of the boundary layer are independent of one another as was assumed in the above estimate.

APPENDIX IV

EFFECT OF SPEED ON WIRE TENSION

The deflection of the wire above a foil was found to be inversely proportional to the wire tension, \underline{T} , and directly proportional to the square of the wire speed, \underline{U}_w [see Equation (14)]. Even under the assumptions made, this is not strictly true because wire tension itself is affected by strains and stresses which vary with speed.

There are a number of forces acting on the running wire to the effect that its tension, \underline{T} , becomes different from the tension \underline{T}_0 which can be measured at rest. The most significant ones are: suction loads, friction in roller bearings and on stationary (foil, scraper) surfaces, centrifugal forces from wrapping the rollers and in following the curvatures of deflections.

Under the operational conditions of the HSHSD and its wire system, the two forces of greatest effect are assumed to be centrifugal forces (at all rolls arranged to change the direction of wire travel) and the suction loads on the wire (wherever these loads cause the wire to be deflected and strained). In order to be able to appreciate their effect on wire tension, the two contributions may be analyzed as follows.

To begin with the centrifugal force, one has for an elemental length $\underline{R}d\phi$ of the wire wrapping a roll of radius \underline{R} , having a thickness δ of a solid space fraction $(1 - \epsilon)$, and made of a material of specific mass $\underline{\rho}_w$, a differential contribution \underline{dT}_c to the wire tension of

$$\underline{dT}_c = \underline{\rho}_w \delta (1 - \epsilon) \underline{R} d\phi \frac{\underline{U}_w^2}{\underline{R}} \cos\alpha \quad (50)$$

where α = angle of direction of the centrifugal force measured from the horizontal, i.e., the direction of wire tension. The total contribution, ΔT_c , is obtained by integrating over the wrapping angles of a representative half portion of the wire-roll system. It could be shown that for any closed-loop system the result becomes

$$\Delta T_c = 2\rho_w \delta (1 - \epsilon) U_w^2 \quad (51)$$

In turning now to the effect of wire wrap on wire tension, we realize that for machines with rigid (i.e., nonfloating) wire-tension adjustment devices wrapping is possible only if, as a consequence of additional stresses, the wire were strained to a greater length. Then, in turn, if the elongation, ΔS , of the wire is known and assumed to be elastic, we may easily obtain the associated stress by means of Hooke's law, which may be written as follows:

$$\Delta T_w = \delta (1 - \epsilon) E \Delta S / L_1 \quad (52)$$

where $\Delta S / L_1$ = wire tension at an original length L_1 , and E = elasticity modulus of the wire screen for the direction of strain. For the length element, dS , of a wire screen under moderate deflections according to Equation (14) (i.e., between two consecutive foils), one has

$$dS \approx [1 + 0.5(h')^2] dx \quad (53)$$

where $h' = dh/dx$. By integrating over the entire length, L_1 , as defined in Fig. 15,

$$\Delta S / L_1 = 0.5 \int_0^{L_1} (h')^2 d(x/L_1) \quad (54)$$

results. By use of Equation (14) and upon change of variable,

$$\Delta S/L_1 = \left(\frac{\rho U_w^2 L_1}{T} \right)^2 \sigma(\kappa, \tau, \lambda)$$

with

$$\sigma = \frac{1}{2} \int_0^L \left\{ \left[\int_0^L f dx dx + (L_1 - L) \int_0^L f dx \right] \frac{1}{L_1^2} - \int_0^L f d\xi \right\}^2 d\xi$$

(55)

is obtained, and with \underline{T} as the real wire tension according to

$$T = T_0 + \Delta T_c + \Delta T_w \quad (56)$$

In the case where there are more than one pair of foils, the right side of Equation (55) must be multiplied by \underline{n}_f = number of pairs of equally distant foils. Before entering the strain (55) into Hooke's law in order to calculate the associated stress, ΔT_w , we assume that the dependence of σ on wire tension [by virtue of $f(\xi)$ as solution of Equation (19)] would be weak as compared with $(1/\underline{T})^2$. Then the right-hand side of the equation for ΔT_w ,

$$\Delta T_w (T_0 + \Delta T_c + \Delta T_w)^2 \approx \delta (1 - \epsilon) E n_f (\rho U_w^2 L_1)^2 \sigma \quad (57)$$

may be treated as a constant. Assuming $\Delta T_w / (T_0 + \Delta T_c) \ll 1$, an approximate root is easily found, and by (55) and considering (57), the wire tension of the running wire is obtained as

$$T = T_0 + 2\rho_w \delta (1 - \epsilon) U_w^2 + \frac{\delta (1 - \epsilon) E n_f (\rho U_w^2 L_1)^2 \sigma}{[T_0 + 2\rho_w \delta (1 - \epsilon) U_w^2]^2} \pm \dots \quad (58)$$

The quantitative significance of the third-order-and-higher terms depends on \underline{n}_f and σ , which latter carries, by Equation (19), the dependence on drainage resistance \underline{K} , foil geometry, etc. No effort was made to evaluate this term because for the system under study it becomes hardly very significant.

Equation (58) would indicate that centrifugal acceleration contributes most strongly to increase in wire tension, while the combined initial and centrifugal tensions would tend to diminish the effect of suction loads. The 80 x 80 flat warp wire screen in use has a basis weight $\underline{w} = \underline{g}_w \delta (1 - \epsilon) = 4 \text{ oz./ft.}^2$, and the wire tension increase according to Equation (51) becomes $\Delta \underline{T}_{\underline{c}} = 0.059 \text{ kg}_f/\text{cm.}$ at a wire speed $\underline{U}_{\underline{w}} = 1000 \text{ f.p.m.}$ and $\Delta \underline{T}_{\underline{c}} = 0.53 \text{ kg}_f/\text{cm.}$ at $\underline{U}_{\underline{w}} = 3000 \text{ f.p.m.}$ This is in the order of less than 3% of most static wire tensions used (7% of wire tension, \underline{G}). Therefore, corrections of the data by use of Equation (58) have been omitted altogether. Obviously, corrections must be applied when experimenting in higher speed ranges (3000 f.p.m. and greater).